

# AUTOMATED 3D SEGMENTATION ON POST-TREATMENT GLIOMA

## Introduction

Gliomas are the most prevalent and fatal primary brain tumors, with high genetic and phenotypic diversity. Automated segmentation of post-treatment glioma MRI scans is essential for monitoring tumor progression, distinguishing recurrence from treatment effects, and developing personalized treatment strategies. The 2024 BraTS (Brain Tumor Segmentation) challenge provided post-treatment glioma multiparametric MRI scans to advance automated MRI segmentation and integrate these models into clinical practice [1].

### Dataset Overview

- Multiple Timepoints per Patient:** The varying number of MRI scans per patient complicates data consistency and analysis.
- Class Imbalance:** The background often dominates the image, complicating accurate identification of smaller target areas.

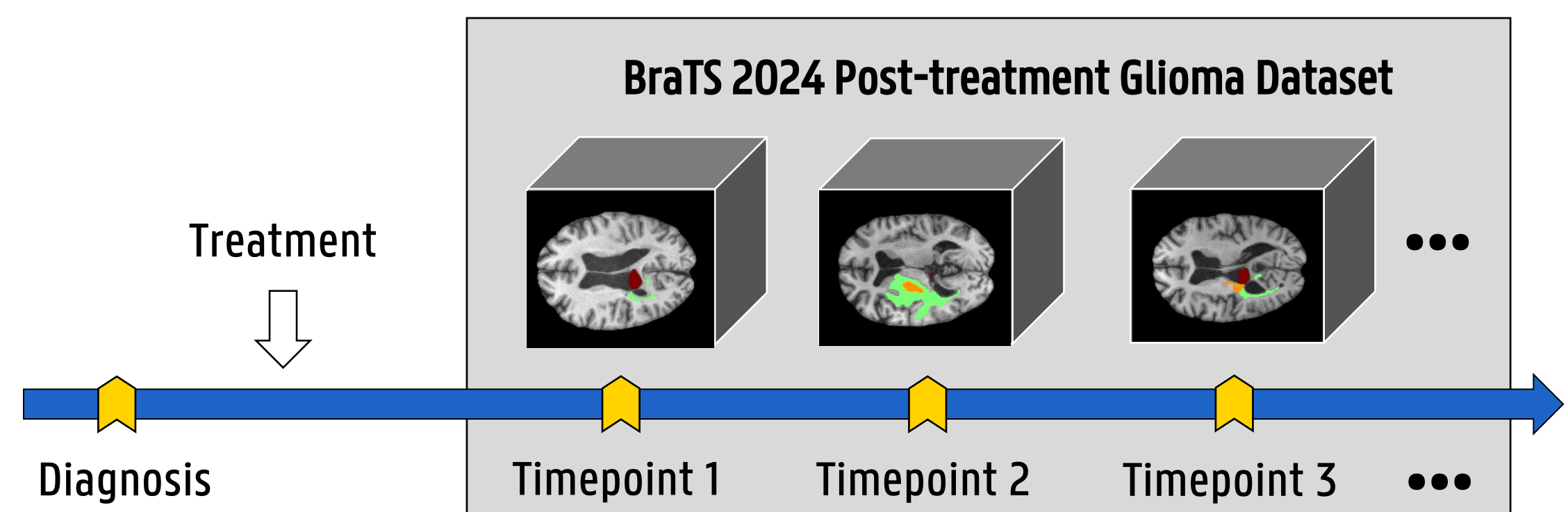


Figure 1: A timeline diagram illustrating the progression of a patient's MRI scans across multiple timepoints in the BraTS 2024 Adult Glioma Post-Treatment Dataset [1].

### 3D Segmentation on Brain MRI

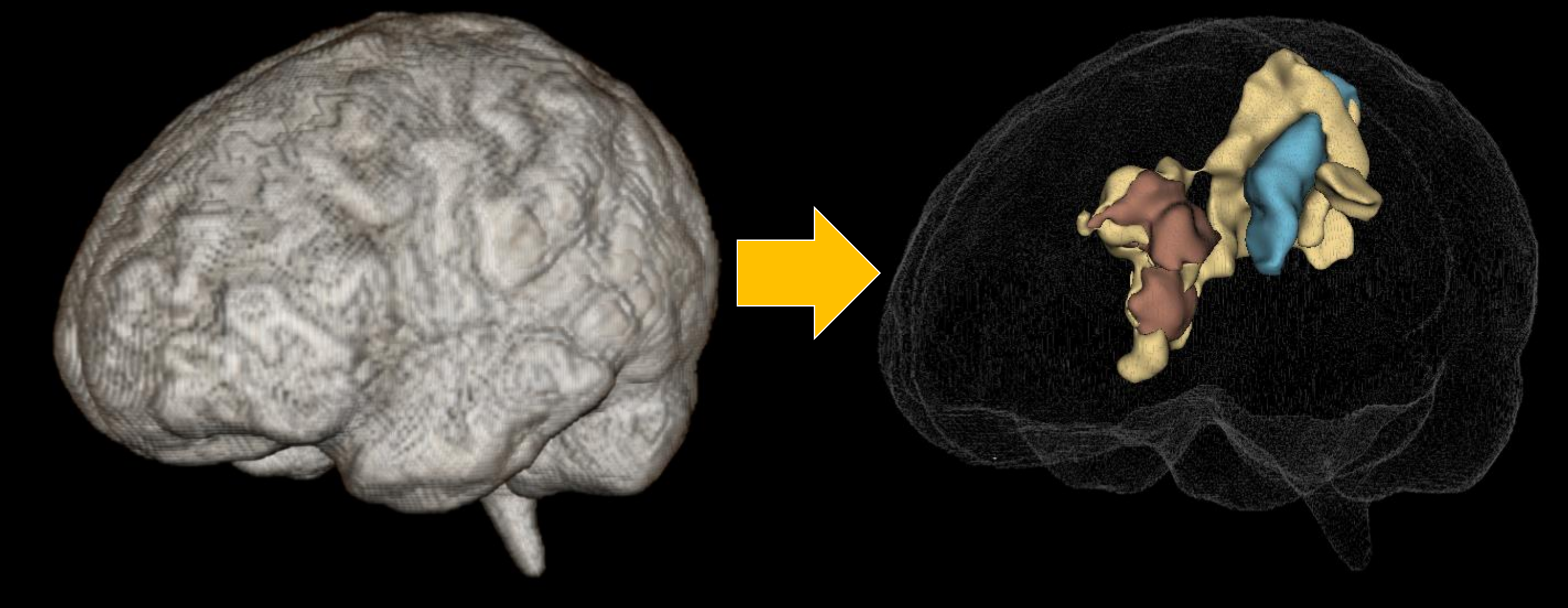


Figure 2: Visualization of a 3D brain MRI volume and its corresponding segmentation labels

### Methodology

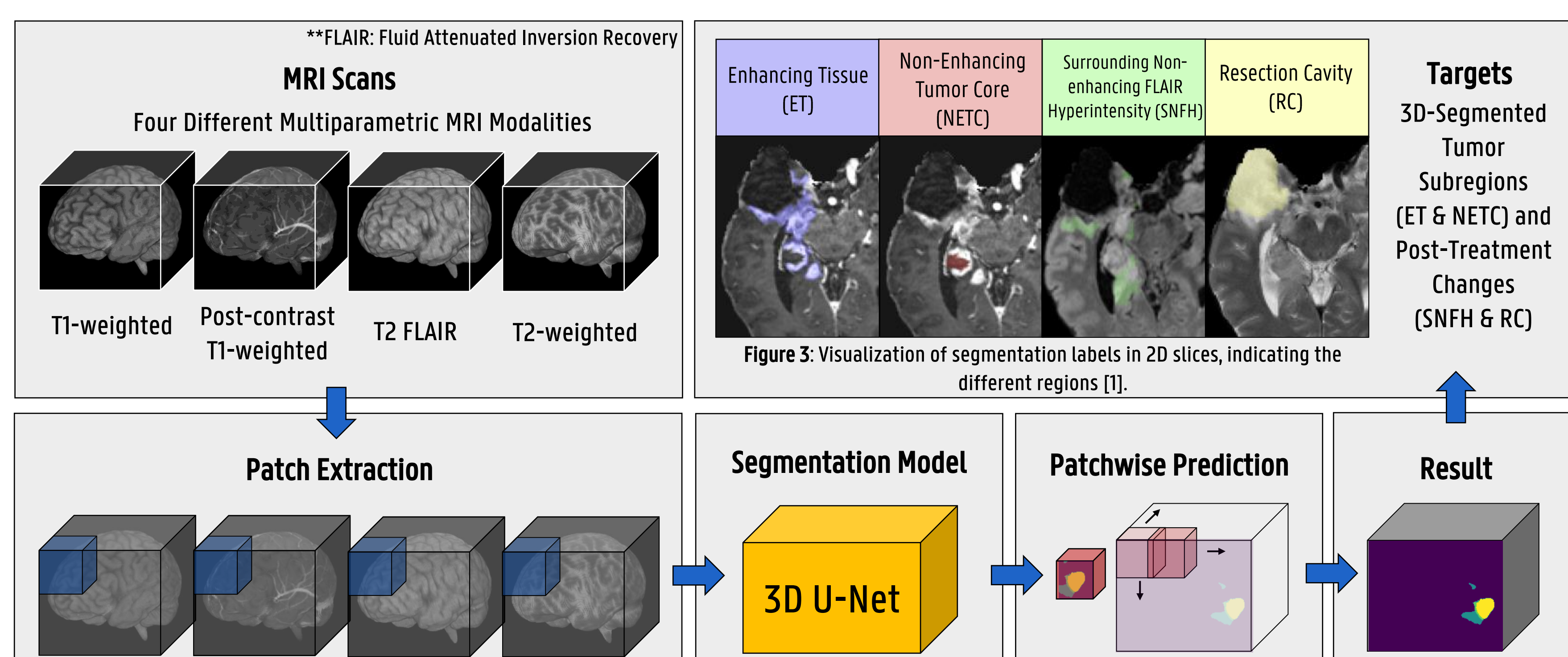


Figure 4: The segmentation workflow starts with combining four MRI modalities into a multichannel 3D object, followed by extracting 96<sup>3</sup> patches for training the 3D U-Net model, and validation using a sliding window approach.

### Results

Dice Score ↑	ET	NETC	SNFH	RC
3D U-Net	0.9248	0.0112	0.9474	0.8495
Winner	0.9738	0.0905	0.9831	0.9378
Hausdorff Distance 95% ↓	ET	NETC	SNFH	RC
3D U-Net	1.4142	31.064	1.4142	5.0990
Winner	1.0000	39.810	1.0000	1.0000

Table 1: Tables comparing dice scores and Hausdorff distance at 95th percentile between the challenge winner's model and 3D U-Net model for each lesion type.

- Dice Score:** Higher for the winner's model.
- Hausdorff Distance 95% (HD95):** Lower for 3D U-Net.
- Small NETC Volume:** Affected segmentation accuracy.
- Trade-off:** 3D U-Net had better boundary precision; winner's model captured lesion volumes better.

### Lesion-wise Overlay of Segmentation Results: Ground Truth, Challenge Winner, and 3D U-Net

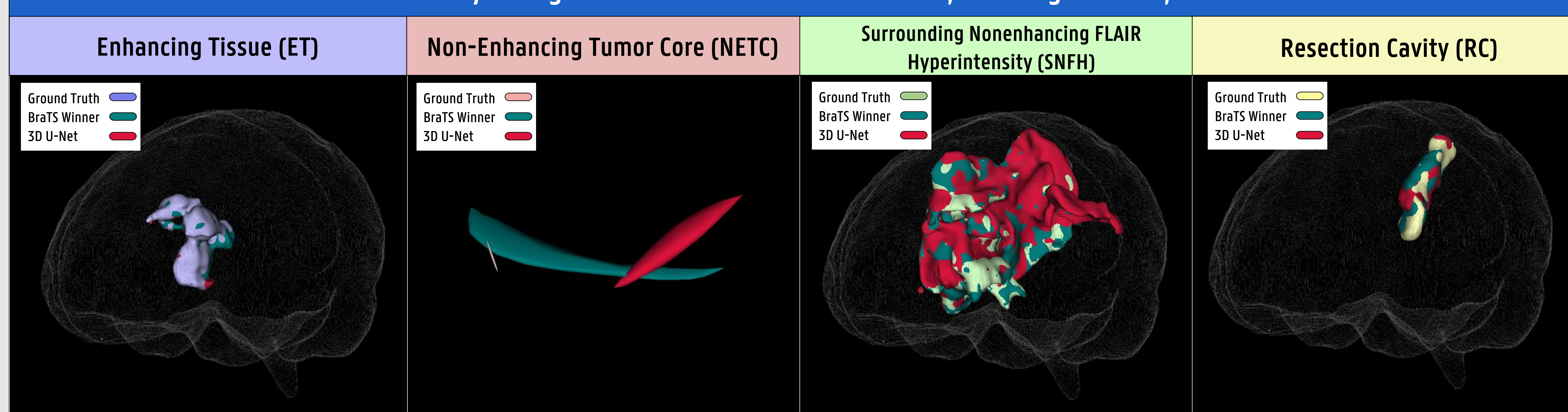


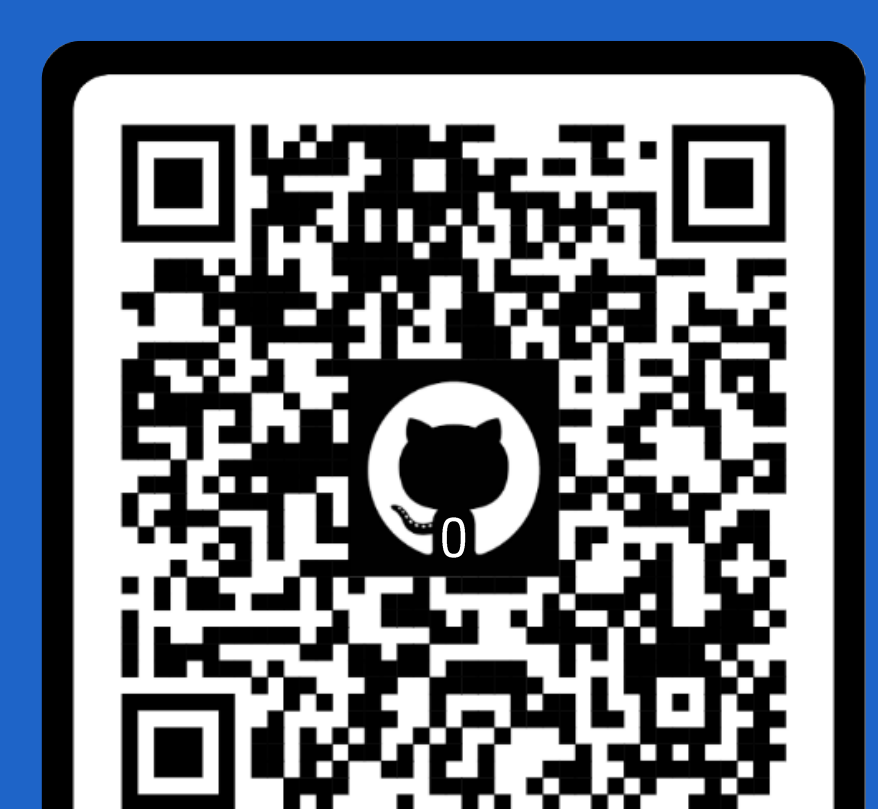
Figure 5: Overlayed segmentations from Ground Truth, the Challenge Winner's Model, and the MONAI-based 3D U-Net Model for four classes (ET, NETC, SNFH, RC), with color coding for each model. NETC segmentation is zoomed in due to the lesion's small area.

## Conclusion

The results highlight a trade-off between boundary precision (HD95) and volume overlap (Dice score) in glioma segmentation. While the 3D U-Net model showed better spatial localization for Non-Enhancing Tumor Core (NETC), the BraTS 2024 Challenge winner's model—based on Hybrid Deep Learning models with synthetic data augmentation (GAN) [2]—achieved higher Dice scores, indicating superior volumetric segmentation. Future work will focus on 5-fold cross-validation training to improve model robustness and developing a real-time interactive segmentation tool for better visualization and analysis. Additionally, I am joining a team for the BraTS 2025 Challenge as part of a team.

## Contact

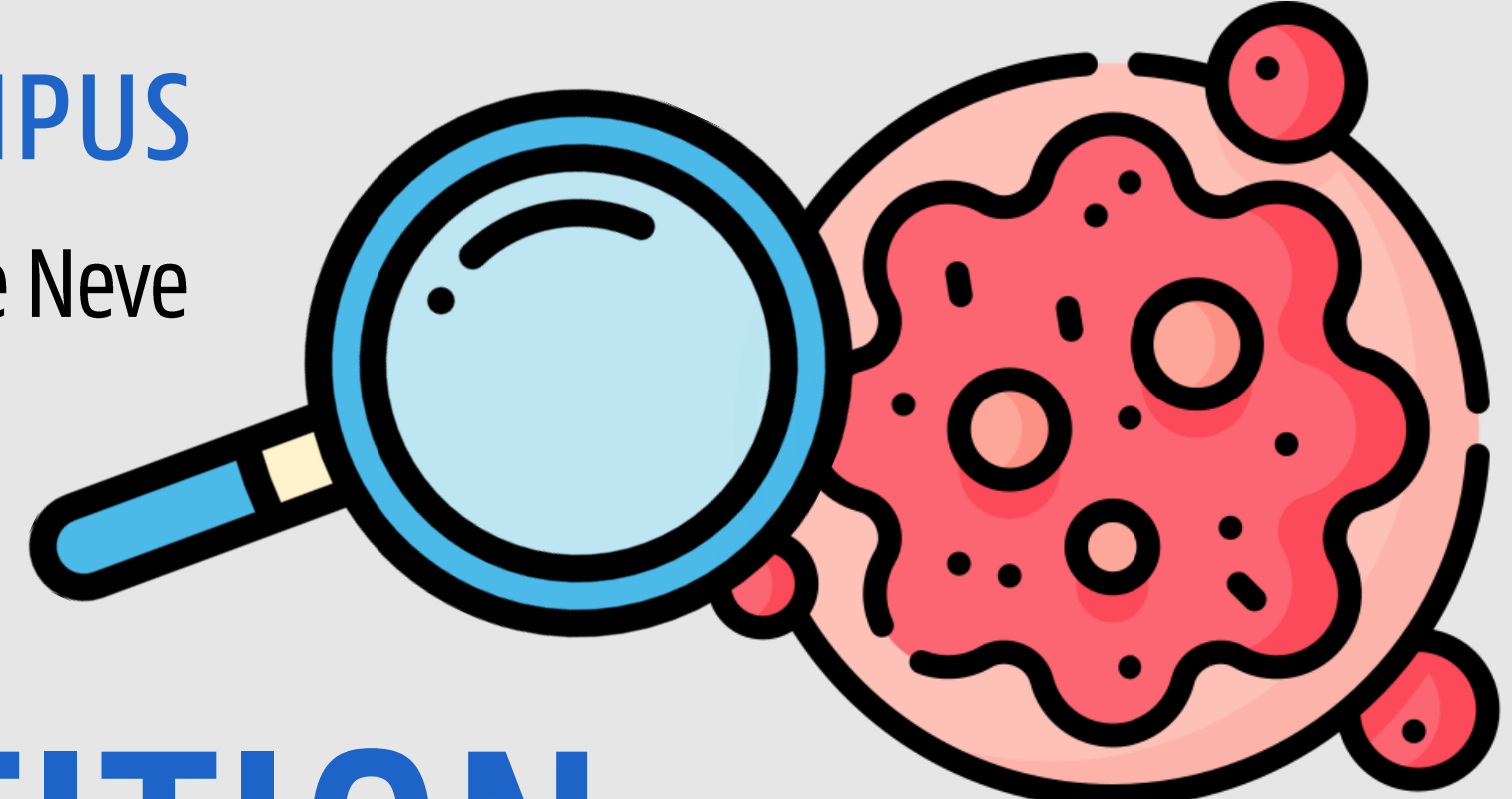
eugekim.Kim@ghent.ac.kr



Code and PPT

### References:

- Verdier, M.C., Saluja, R., Gagnon, L., Labelle, D., Baid, U., et al. (2024). The 2024 Brain Tumor Segmentation (BraTS) Challenge: Glioma Segmentation on Post-treatment MRI. ArXiv, abs/2405.18368.
- Ferreira, A., Jesus, T., Puladi, B., Kleesiek, J., Alves, V., & Egger, J. (2024). Improved Multi-Task Brain Tumour Segmentation with Synthetic Data Augmentation. ArXiv, 2411.04632.



# MULTI-CLASS IMAGE CLASSIFICATION: PAP SMEAR CELL CLASSIFICATION COMPETITION

## Introduction

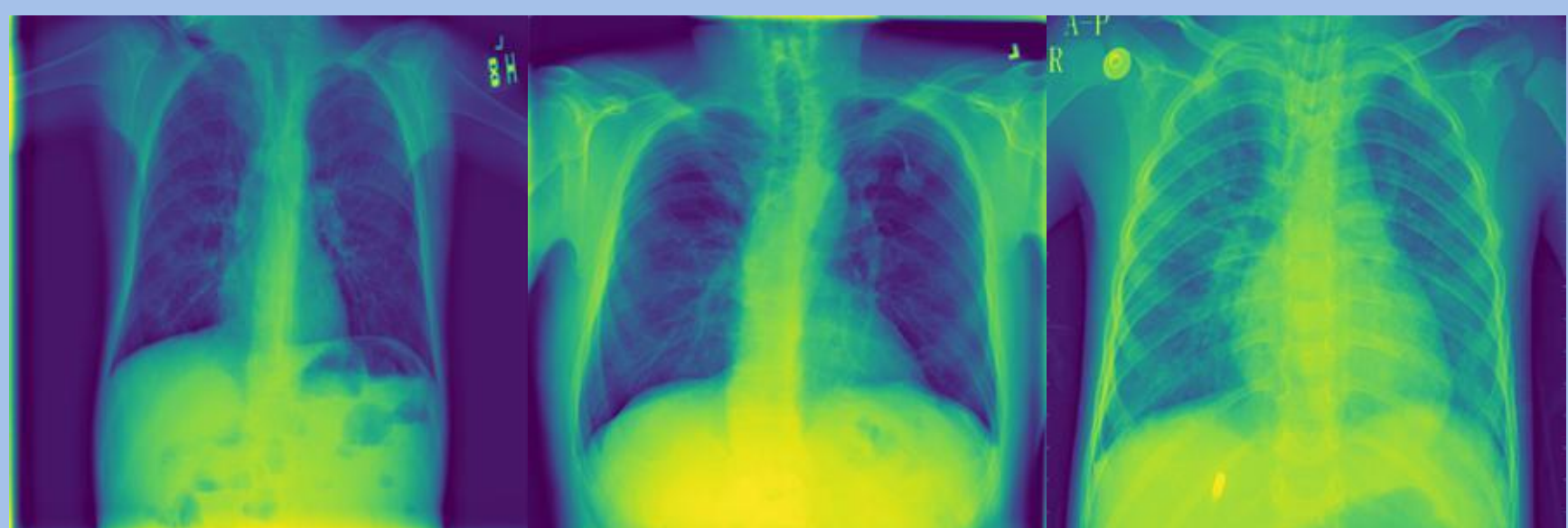
As part of the ISBI 2025 challenges, this competition aims to enhance cervical cancer screening through AI-driven Pap smear cell classification. The 5-year relative survival rate for localized cervical cancer is 91%, but it drops sharply to 19% once the cancer has spread distantly (ACS, 2025). This highlights the critical importance for early detection in increasing survival rates. However, many uninsured and low-income women face barriers to regular screenings, leading to disparities in early diagnosis and treatment. AI-powered solutions can help to bridge this gap by making Pap smear test more accessible and efficient, ultimately advancing cancer detection and patient outcomes.

Dataset Details			Machine Learning Model Performance																				
Train set (4 classes): 85080 images																							
Test Set (3 classes): 18159 images																							
			<b>(A) Feature Extraction</b>  Evaluation Metric: F1-score		<table border="1"> <thead> <tr> <th>Model</th> <th>5-fold Cross Validation</th> <th>Submission Score</th> </tr> </thead> <tbody> <tr> <td>Logistic regression</td> <td>0.99756</td> <td>0.79082</td> </tr> <tr> <td>Random forest</td> <td>0.99704</td> <td>0.80756</td> </tr> <tr> <td>Gradient boosting</td> <td>0.99699</td> <td><b>0.81615</b></td> </tr> <tr> <td>Support Vector Machine</td> <td>0.99766</td> <td></td> </tr> <tr> <td>Multi-Layer Perceptron</td> <td>0.99741</td> <td></td> </tr> </tbody> </table>	Model	5-fold Cross Validation	Submission Score	Logistic regression	0.99756	0.79082	Random forest	0.99704	0.80756	Gradient boosting	0.99699	<b>0.81615</b>	Support Vector Machine	0.99766		Multi-Layer Perceptron	0.99741	
Model	5-fold Cross Validation	Submission Score																					
Logistic regression	0.99756	0.79082																					
Random forest	0.99704	0.80756																					
Gradient boosting	0.99699	<b>0.81615</b>																					
Support Vector Machine	0.99766																						
Multi-Layer Perceptron	0.99741																						
<b>Feature Selection</b>			<b>Optimized ANN training via Feature Selection</b>																				
Set thresholds for each model based on the feature importance			After feature selection, the score surpassed 0.85, exceeding the baseline.																				
<ul style="list-style-type: none"> <li>✓ Gradient boosting: Removed all features with zero importance</li> <li>✓ Random forest &amp; Logistic Regression: Utilized visual inspection</li> </ul> ▲ Random Forest Feature Importance Distribution    ▲ Logistic Regression Coefficient Distribution			<b>(B) Feature Selection</b>  <b>(C) Training</b> <table border="1"> <thead> <tr> <th>Selected by</th> <th>Submission Score</th> </tr> </thead> <tbody> <tr> <td>Logistic regression</td> <td>0.85020</td> </tr> <tr> <td>Random forest</td> <td><b>0.85031</b></td> </tr> <tr> <td>Gradient boosting</td> <td>0.85007</td> </tr> </tbody> </table>			Selected by	Submission Score	Logistic regression	0.85020	Random forest	<b>0.85031</b>	Gradient boosting	0.85007										
Selected by	Submission Score																						
Logistic regression	0.85020																						
Random forest	<b>0.85031</b>																						
Gradient boosting	0.85007																						
Explainable AI																							
The SHAP summary plot revealed that <b>feature_10</b> has the highest impact magnitude. Based on its level, there is a significant difference within the group.																							
		<b>High</b>  <ul style="list-style-type: none"> <li>✓ Large cells with rich cytoplasm</li> <li>✓ Intense red/blue staining with clear nuclear boundaries</li> </ul>	<b>Low</b>  <ul style="list-style-type: none"> <li>✓ Dark-centered large cells with indistinct borders</li> <li>✓ Intense dark blue/purple staining</li> </ul>																				
Improvement			 rubbish   healthy   both cells   unhealthy																				
The dataset was highly imbalanced, reflecting real-world conditions. Preprocessing to balance the dataset could significantly enhance performance. Additionally, we should compare our approach with top-ranking solutions for further evaluate improvements.			 GitHub / Paper																				
Competition Results			Contact																				
Preliminary phase: 14 <sup>th</sup> out of 41 teams (0.85227), Final evaluation: 12 <sup>th</sup> out of 16 teams (0.72305)			 Slides																				

# AI-DRIVEN PNEUMONIA CLASSIFICATION FROM MEDICAL X-RAYS

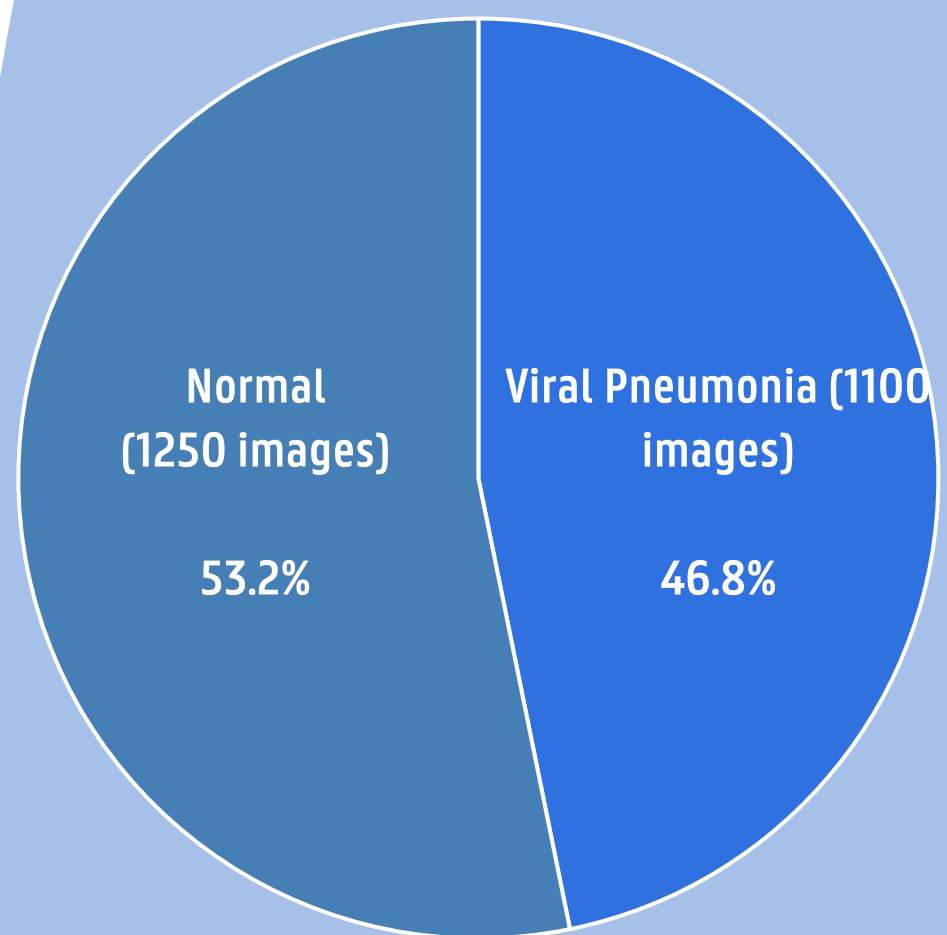
Pneumonia is a widespread infectious disease and a leading cause of death worldwide. While it is highly treatable with early diagnosis, a shortage of doctors in certain regions makes timely detection challenging. This study explores the use of an AI-driven model, DenseNet161, to analyze lung X-ray images for detecting viral pneumonia. By leveraging AI for fast and accurate diagnosis, this approach aims to improve early detection and enhance healthcare efficiency.

## 1. Dataset: Lung X-ray Images



To train and test a model that analyzes lung X-ray images, a dataset with such X-ray images was chosen. As seen from the sample X-rays above, this dataset is a collection of high-quality images from healthcare institutions.

## Dataset Analysis - Distribution of Images



The dataset consists of X-ray images of lungs, categorized as either normal or affected by viral pneumonia. The normal class contains 150 more images than the pneumonia class, resulting in a mild class imbalance. However, this imbalance has a negligible impact on the model's performance.

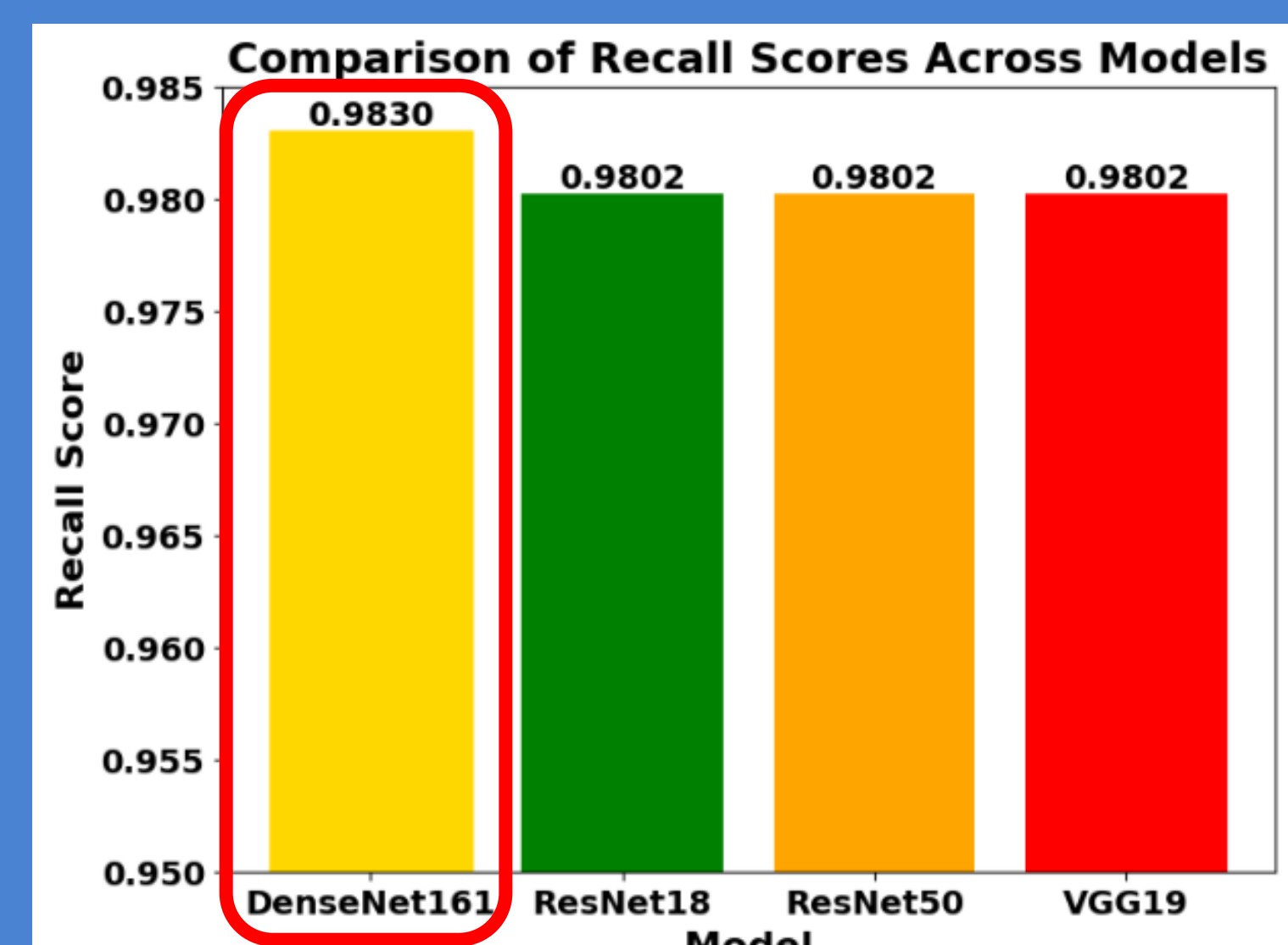
## 3. Comparison of models

Arbitrary AI models other than the DenseNet161 model were selected and trained to determine the most effective model in classifying the dataset as having pneumonia or not. The recall was used for comparison. Recall measures the model's ability to correctly identify positive cases.

$$\text{Recall} = \frac{\text{True Positive}}{\text{True Positive} + \text{False Negative}}$$

**True Positive:** Patient has pneumonia, model correctly predicts it  
**False Negative:** Patient has pneumonia, model predicts as "Normal"

High recall ensures most infected cases are detected, reducing false negatives and preventing undiagnosed disease spread.

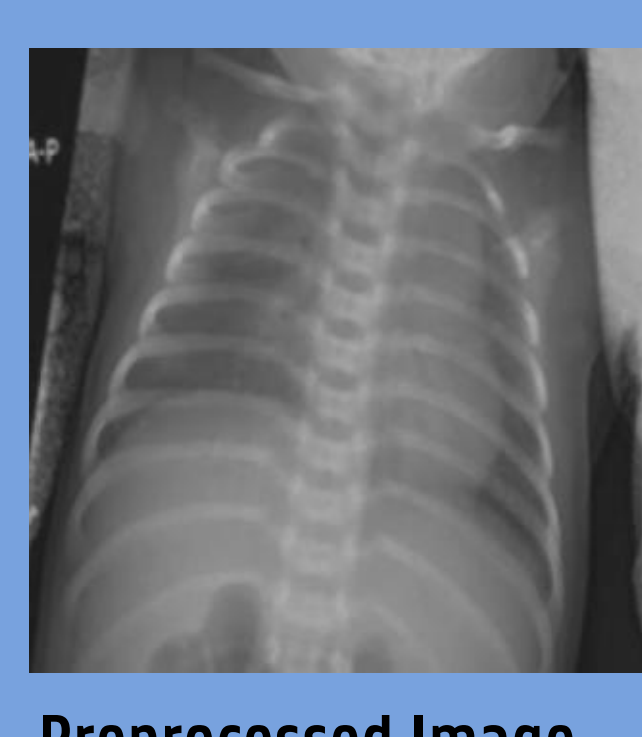
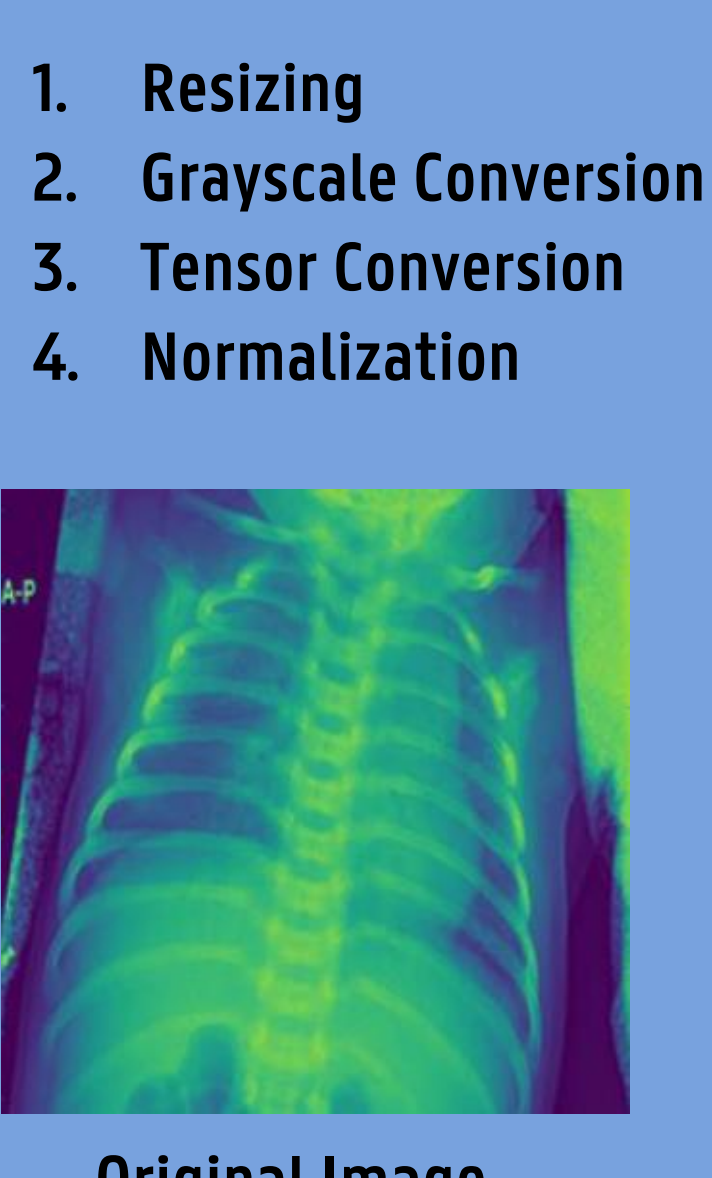


**Densenet161 is the most efficient model**

## 2. Data Preprocessing

For the X-ray images to be interpreted by the AI model to be used, the images must be pre-processed, like preparing ingredients before cooking.

The preprocessing steps the images went through are shown as below:



Original Image

Preprocessed Image

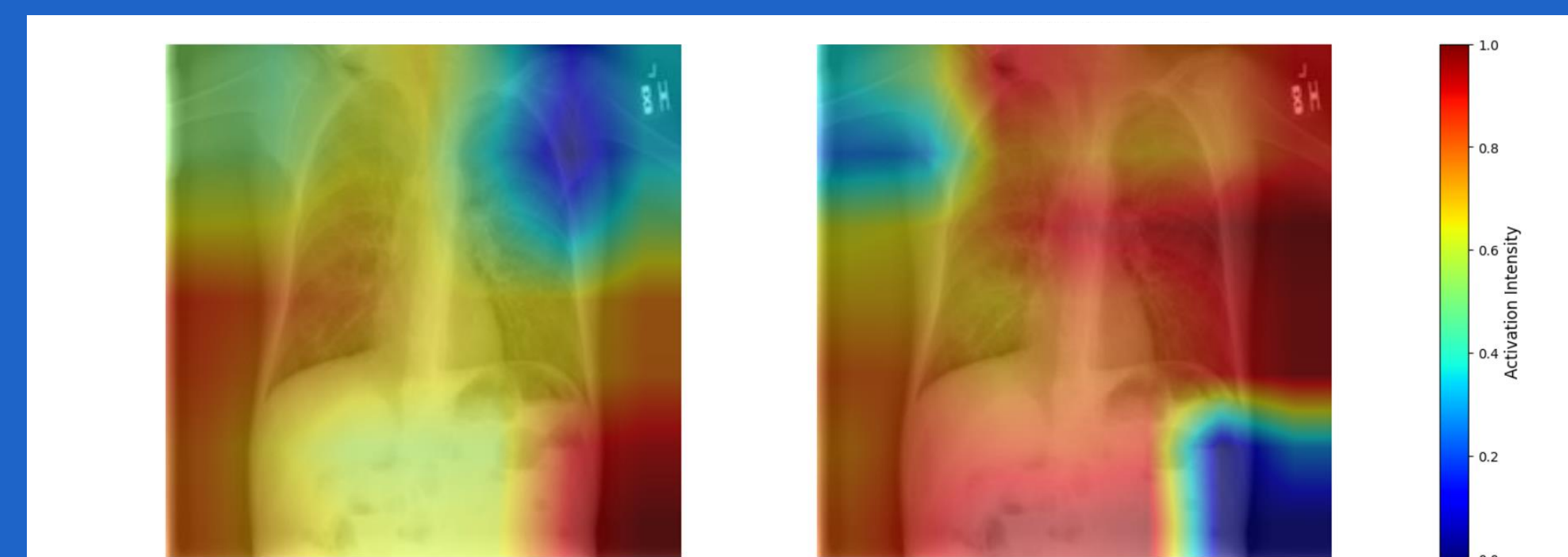
## Model Initialization & Training

DenseNet161 model was used to analyze the X-ray images. DenseNet161 model is a deep CNN with 161 layers that enhances feature reuse through dense connections. This model was initialized by setting its hyperparameters and validation method as below.

**Hyperparameters**  
 Learning rate: 0.001  
 Batch Size: 32  
 Optimizer: AdamW  
 Loss Function: Cross Entropy Loss  
 Epoch: 50

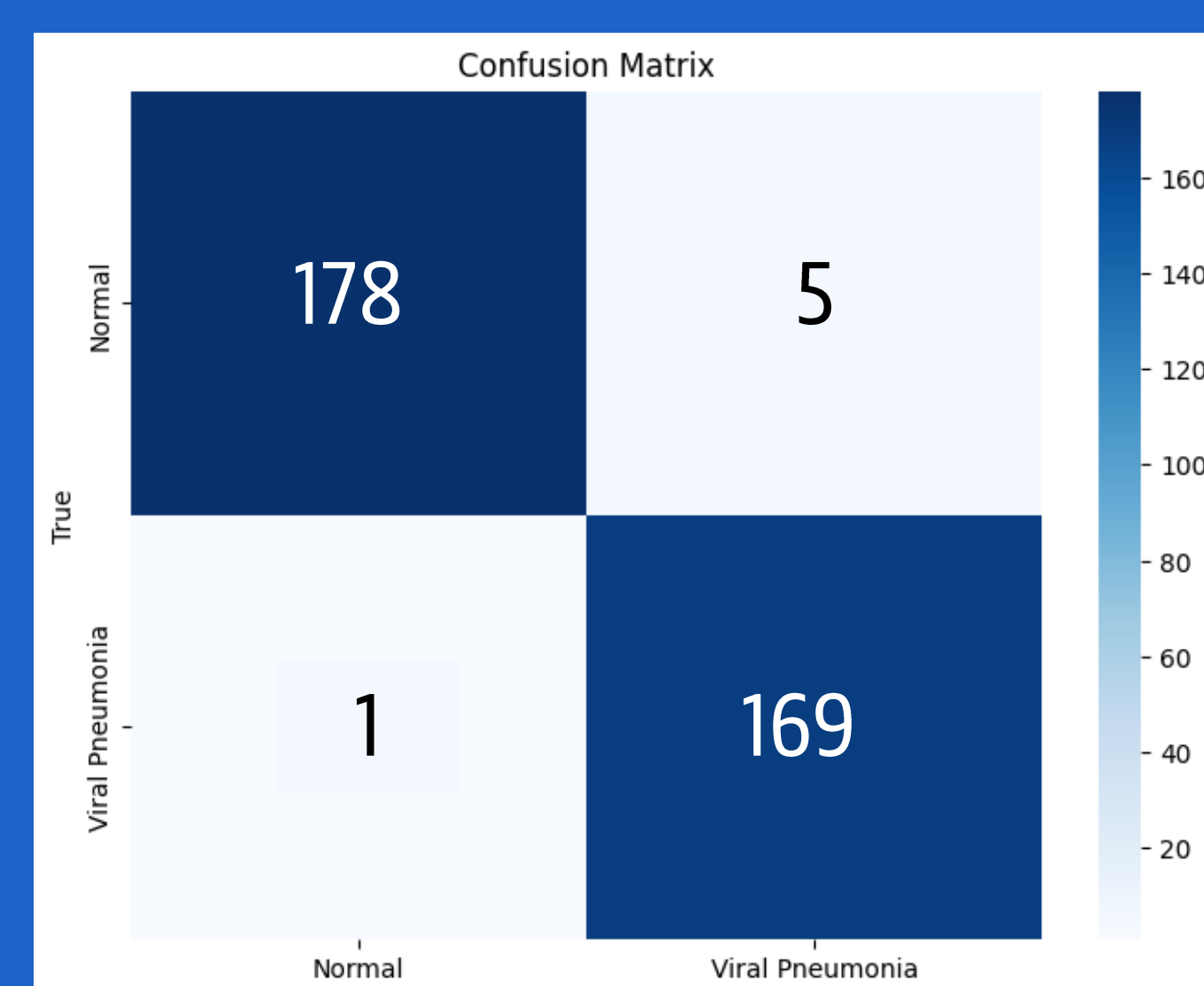
**Holdout Validation**  
 The whole dataset is split into:  
 Training (70%)  
 Validation (15%)  
 Test (15%)

## 4. Results



The thought process of the DenseNet161 model was visualized as can be seen from the above image. Summed Grad-CAM heatmaps were used, showing which regions the model focused overall when deciding whether the lungs had pneumonia (left) or whether the lungs were normal (right). In the case with pneumonia, the model highly focused on the upper chest and lung areas.

## Conclusion



Precision      0.9833  
 Recall      0.9830  
 F1 Score      0.9830

The performance of the DenseNet161 model can be seen below from the confusion matrix. This model obtained a recall score of 0.9830, a very high number, thus it can be concluded that the model effectively classified the given dataset correctly.

The DenseNet161 model successfully identified areas where pneumonia showed the most prominent activity, with a high recall score from the given dataset. Therefore, it can be concluded that the model performed effective classification.





# DETECTING ADULTERATION IN COFFEE USING HYPERSPECTRAL IMAGING AND MACHINE LEARNING

## Introduction

Coffee is majorly divided into 2 bean types: **Arabica** and **Robusta**, and Arabica coffee is often adulterated with Robusta coffee beans to cut costs. The adulteration in the product is indistinguishable once the coffee is ground, posing a persistent challenge in combating food fraud.

This experiment explores the ability of machine learning methods in combination with **Near Infrared Hyperspectral Imaging (NIR-HSI)**. Exploration into this methodology shows potential of a non-destructive and rapid method of assessing Robusta adulteration in Arabica coffee.

## Data Collection

### Part 1: From Coffee Beans to Instant Coffee

Independently sourced Arabica and Robusta coffee beans were **roasted**, **brewed**, and **freeze dried** to create instant coffee samples.



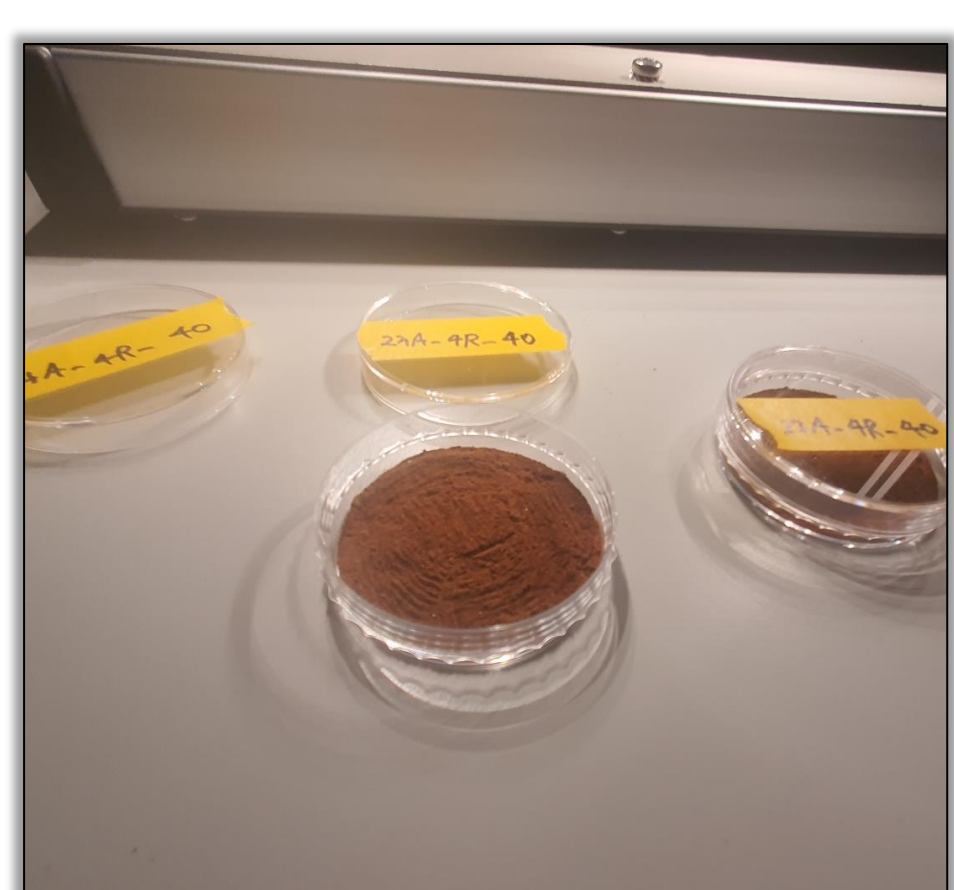
### Part 2: Data Collection using NIR-HSI

By combining known amounts of **Arabica** & **Robusta** coffee, 1-gram samples were made at varying adulteration levels: **0%, 1%, 5%, 10%, 20%, 40%, 60%, 80%, 100%**.

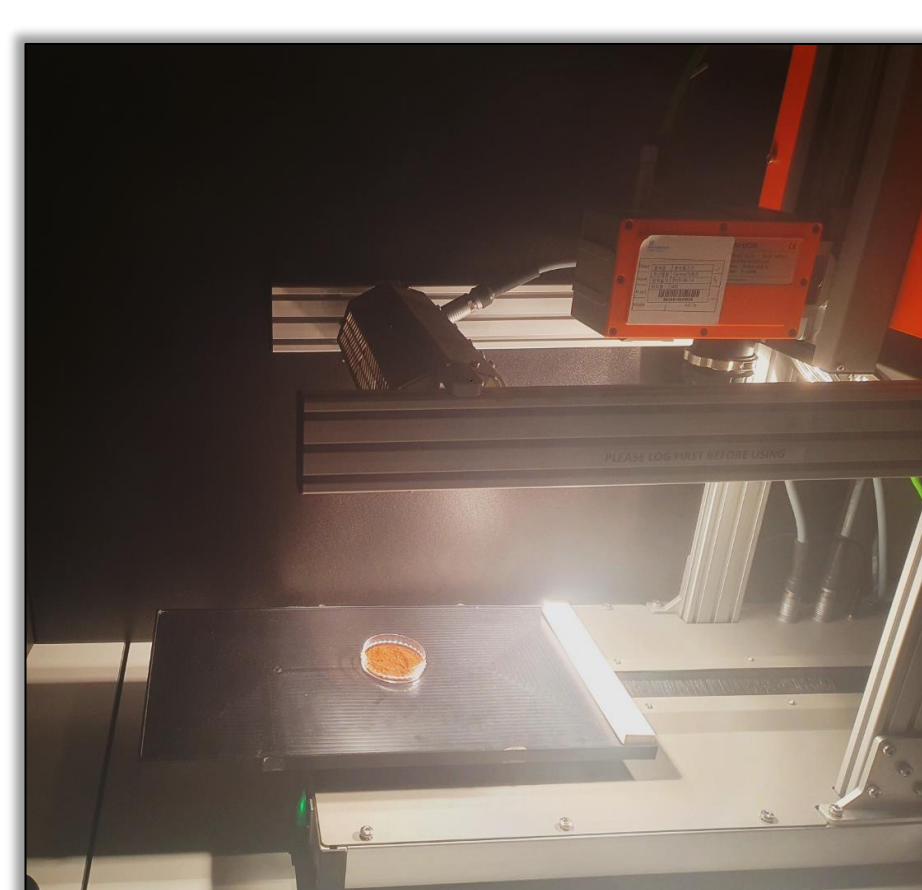
Training & testing sets were created using separate pools of coffee to prevent data leakage. Samples were then individually imaged via NIR-HSI technology.



Creating Sample Mixes



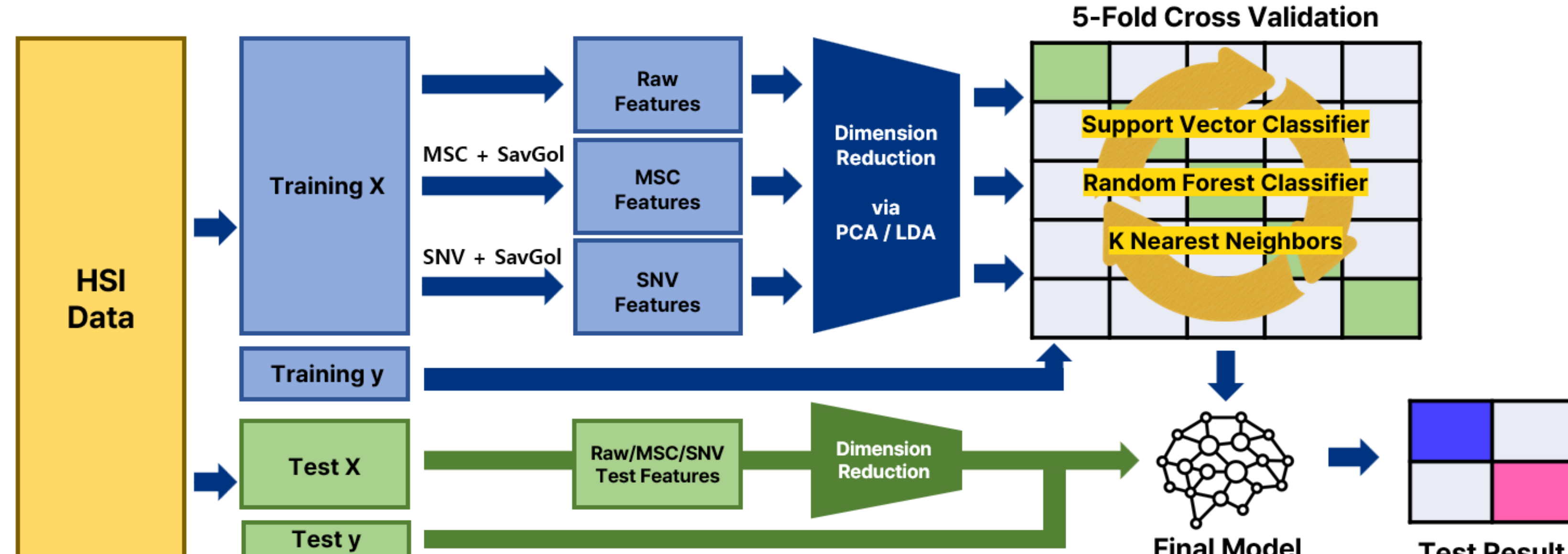
Preparing Sample for HSI



Imaging Process

### Part 3: Applying Machine Learning Methods

The data gained from NIR-HSI underwent **preprocessing & dimension reduction**. This data then went through **5-fold cross validation** with **hyperparameter tuning** to find the best model based on its **F1-score**. The **binary classification model** is evaluated with the test set, outputting a **confusion matrix**.



3 preprocessing functions were applied to the data: **Multiplicative Signal Correction (MSC)**, **Standard Normal Variate (SNV)**, and **Savitzky-Golay Filtering (SavGol)**

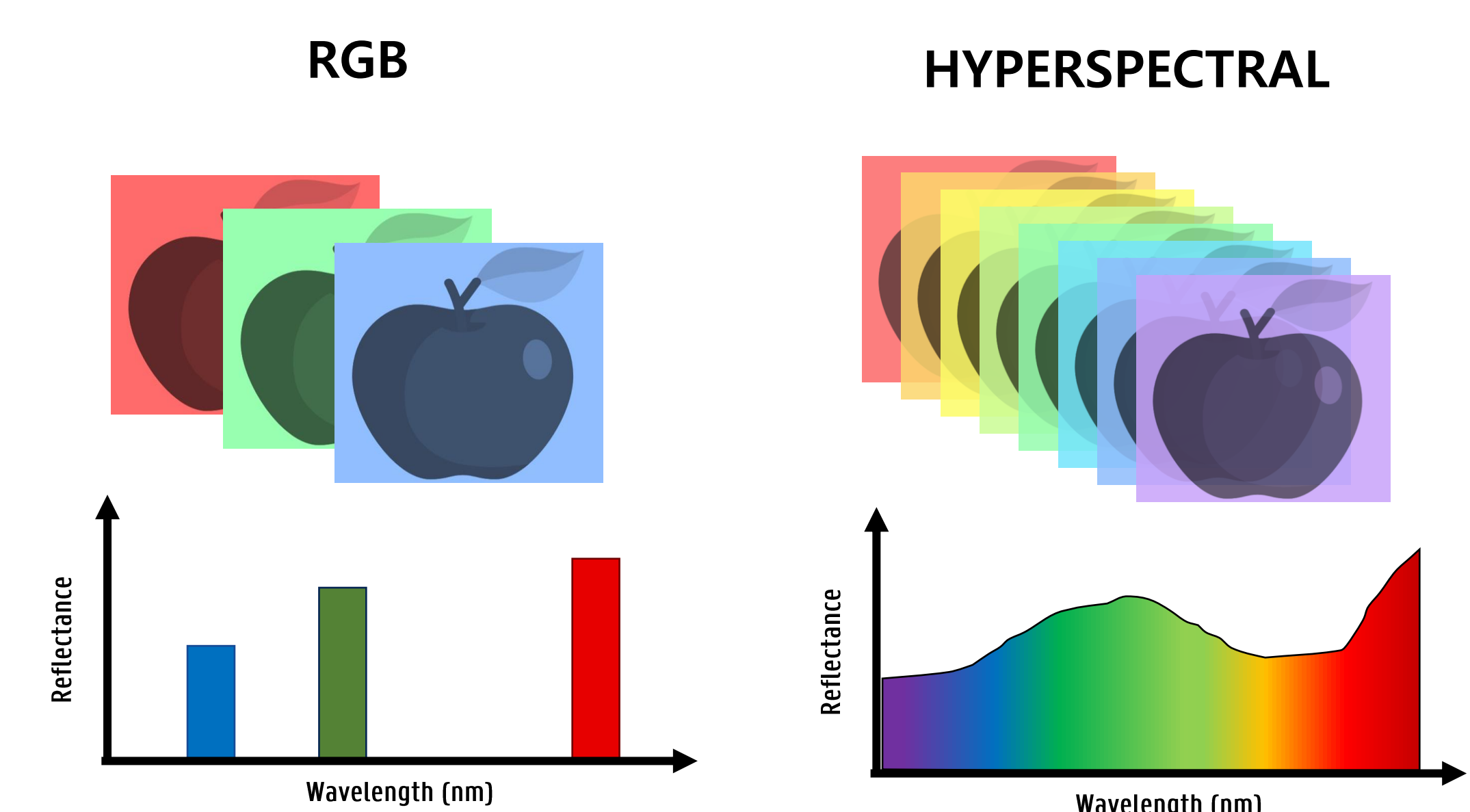
2 dimension reduction methods were then applied: **Principal Component Analysis (PCA)** and **Linear Discriminant Analysis (LDA)**

All 6 combinations of preprocessing and dimensionality reduction were evaluated using **5-fold cross-validation** with multiple classification algorithms.

## Understanding the Data

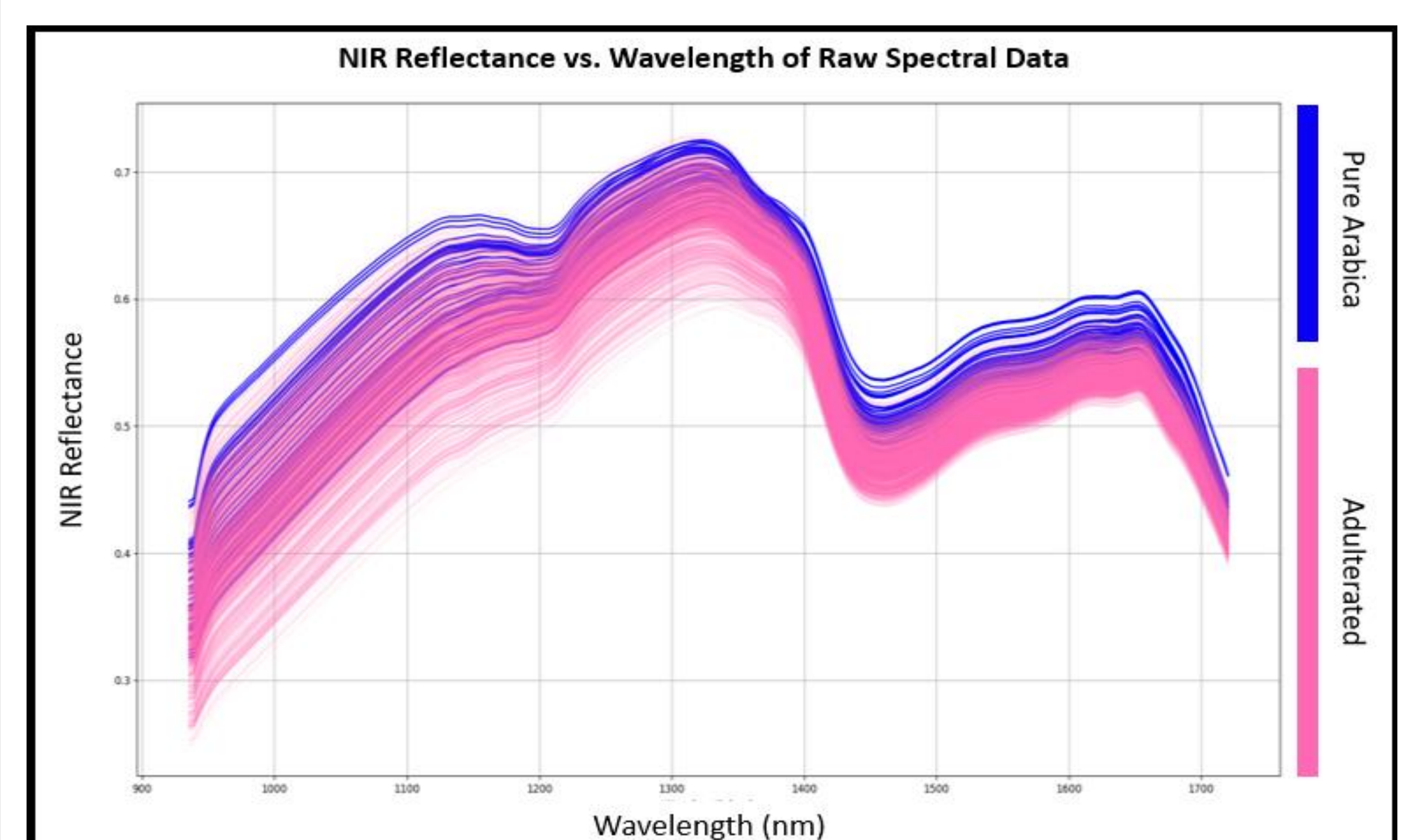
### RGB vs. Hyperspectral

RGB color model uses 3 color bands, while **Hyperspectral Images** use a **continuous spectrum**.



## Data Visualization

Below is a graphical representation of the data, color coded by **Pure Arabica** or **Adulterated** samples.



## Results

### Best Model Outcome:

- MSC/SNV Preprocessing
- LDA Dimension Reduction
- Support Vector Classifier:  $C=1$ , kernel= 'rbf', gamma= 0.01

99.77% accuracy

99.87% F1-score

### Confusion Matrix of the Best Model

		Predicted Label ( $\hat{y}$ )	
		Pure Arabica	Adulterated
True Label ( $y$ )	Pure Arabica	26	1
	Adulterated	0	384

Pure Arabica      Adulterated

## Conclusion

The model correctly classified **410 out of 411** test samples, demonstrating the effectiveness of combining NIR-HSI with appropriate preprocessing and dimensionality reduction techniques for binary classification. These results highlight the potential of this approach for rapid, non-destructive adulteration assessment.

# ENHANCING ALZHEIMER'S DISEASE PREDICTION USING MACHINE LEARNING AND SHAP ANALYSIS



## Introduction

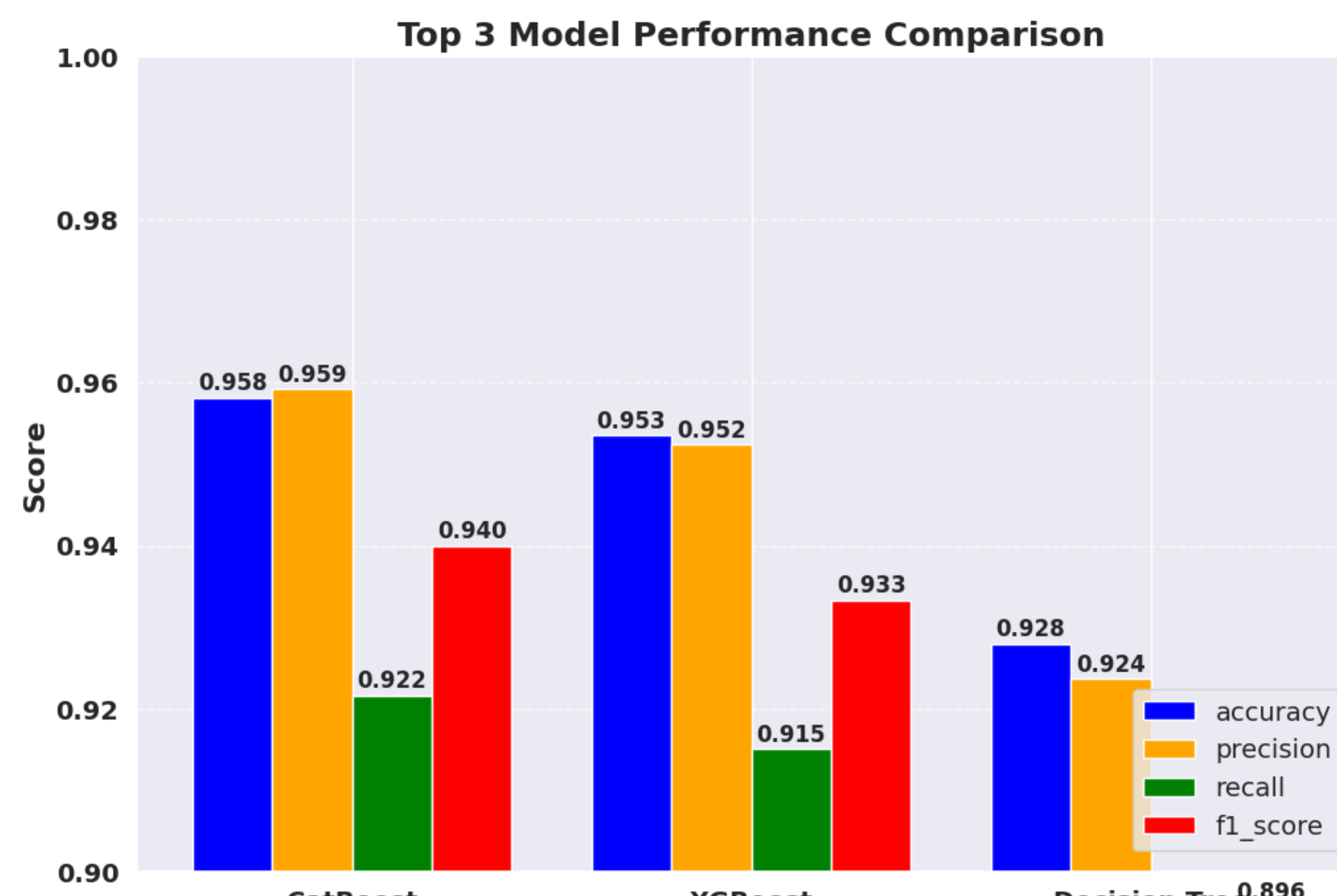
From 2020 to 2050, the economic burden of Alzheimer's disease and other dementias is expected to reach approximately 14.513 trillion international dollars (as of 2020) in 152 countries around the world. In particular, Japan had the highest economic burden of dementia at 1.463% of GDP. In Korea, the economic burden is estimated at approximately 49.6662 trillion won, and the proportion of GDP is 0.686%. In this situation, early diagnosis and prevention of Alzheimer's disease are essential.

### About Dataset

MMSE	21.463532	20.613267	7.356249	13.991127	13.517609
FunctionalAssessment	6.518877	7.118696	5.895077	8.965106	6.045039
MemoryComplaints	0	0	0	0	0
BehavioralProblems	0	0	0	1	0
ADL	1.725883	2.592424	7.119548	6.481226	0.014691
Confusion	0	0	0	0	0
Disorientation	0	0	1	0	0

- Total 2149 dataset
- 35 columns (features)
- Types : 12 float types / 22 int types / 1 object type
- No null data or duplicate records

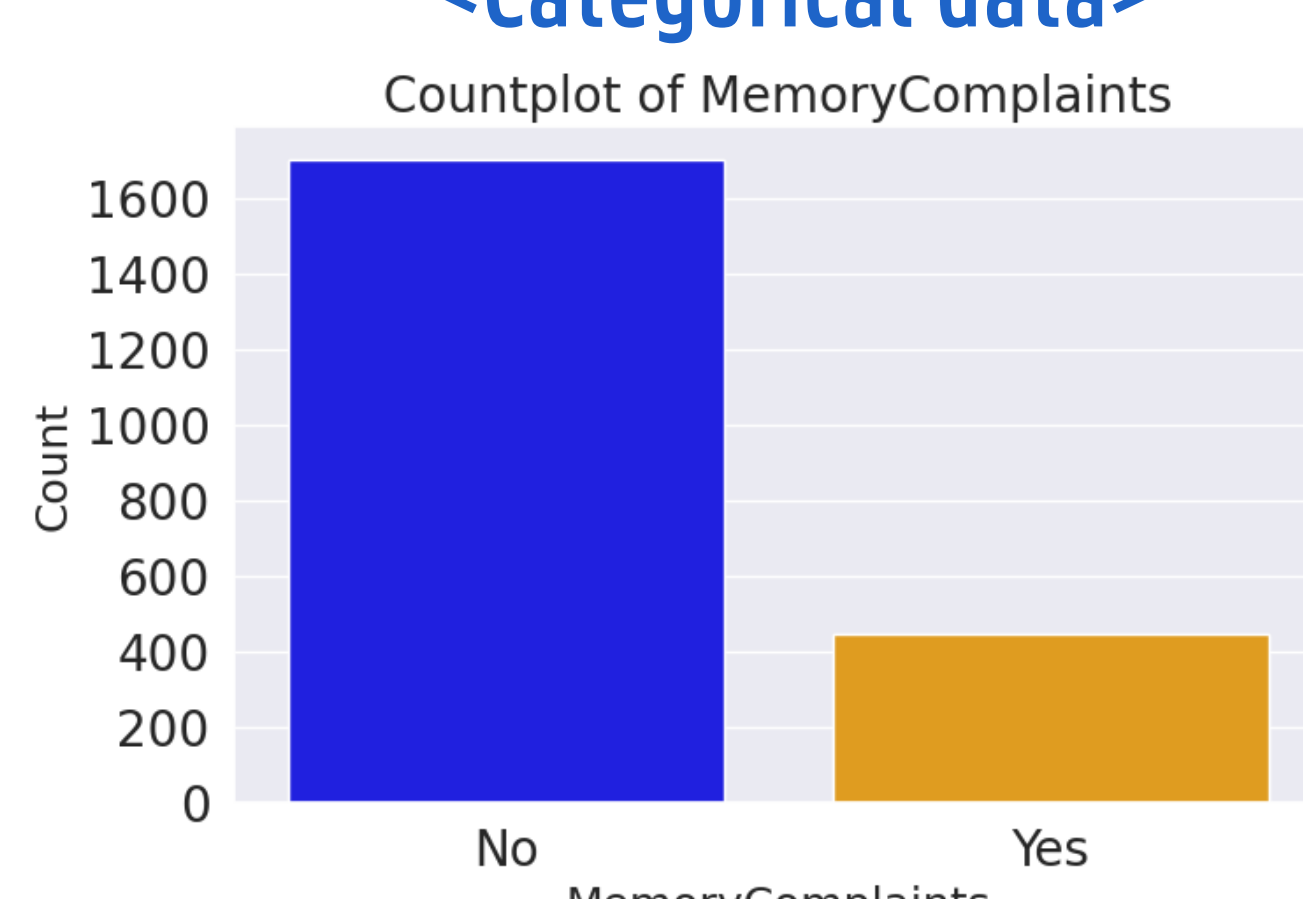
### Modeling Comparison



CatBoost is the most effective machine learning model for reducing **False Negatives** and **False Positives** due to high score of the precision, recall, and f1-score.

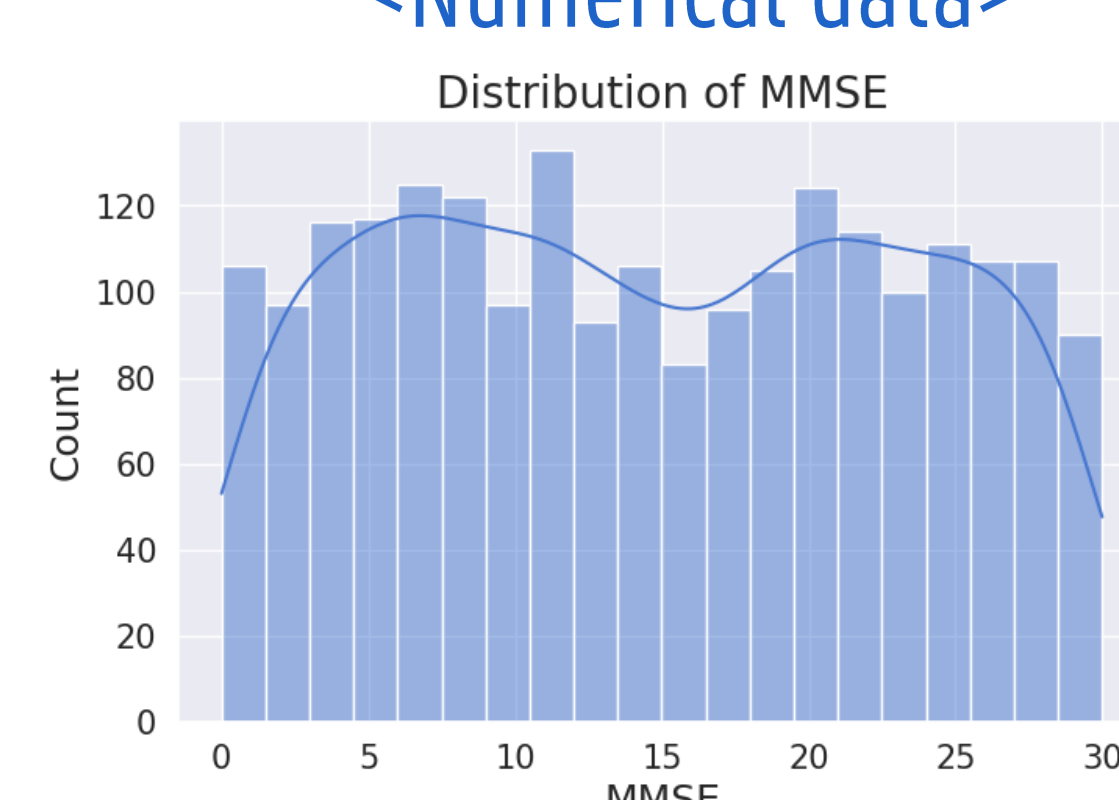
### Data analysis

#### <Categorical data>



The dataset predominantly consists of Individuals **without** disease or healthProblems. (Dataset with **unbalance**)

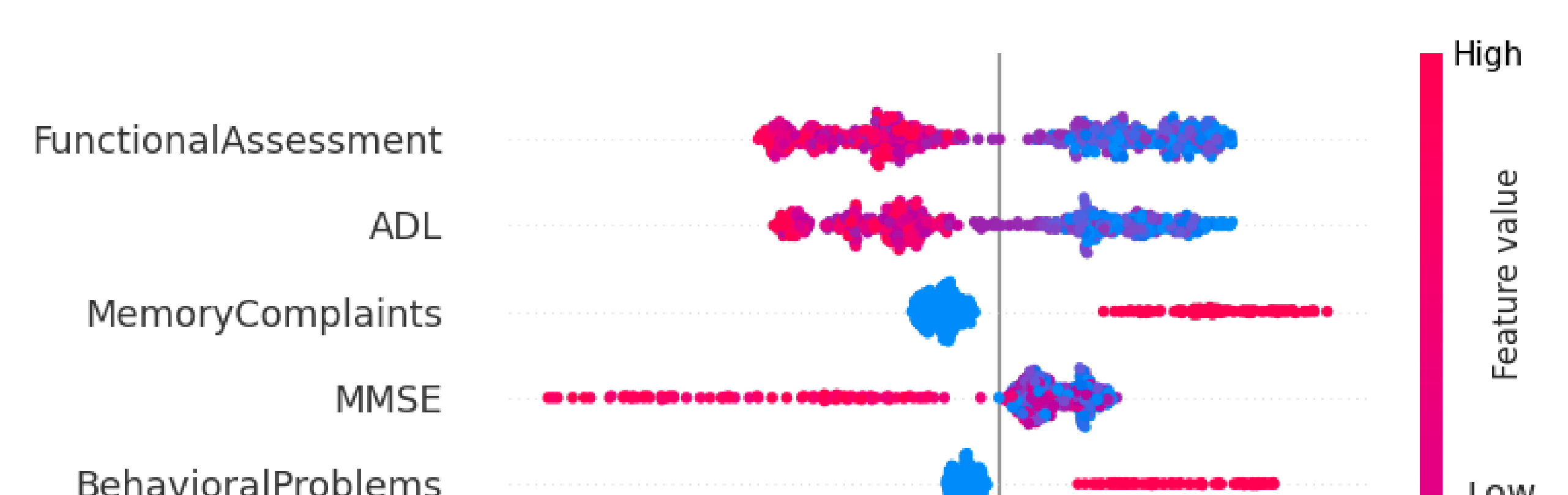
#### <Numerical data>



In case of MMSE feature, it has **bimodal** distribution, which means healthy group and the group with cognitive decline are likely to be **distinguished**.

\* In addition, most relevant variables are MMSE, FunctionalAssessments, ADL (negative correlation), MemoryComplaints, and BehavioralProblems (positive correlation). They show the highest correlation with diagnosis.

### Feature importance : SHAP



- Behavioral problems, Memory complaints with **narrow** SHAP values
    - small effect on the prediction and are **not** heavily relied on by the model
  - Functional assessment, ADL, and MMSE with **wide** SHAP values
    - these variables **strongly** changes the model's prediction
- SHAP allows modeling by selecting the most relevant variables and giving them a higher weight in the next prediction.

### Conclusion

1. **CatBoost** is the most suitable model for predicting Alzheimer's. If this model is used for early diagnosis of suspected patients in the future, the prediction probability will be the highest.
2. Results by SHAP are similar even after removing the bottom 20% of variables. It means that the model relies on key variables, and was **trained without relying on unnecessary variables** (Noise). Therefore, the generalization performance is likely to be high.

### Contact

Junhui.Lee@ugent.ac.kr

Universiteit Gent

@ugent

Ghent University

<PPT Link>



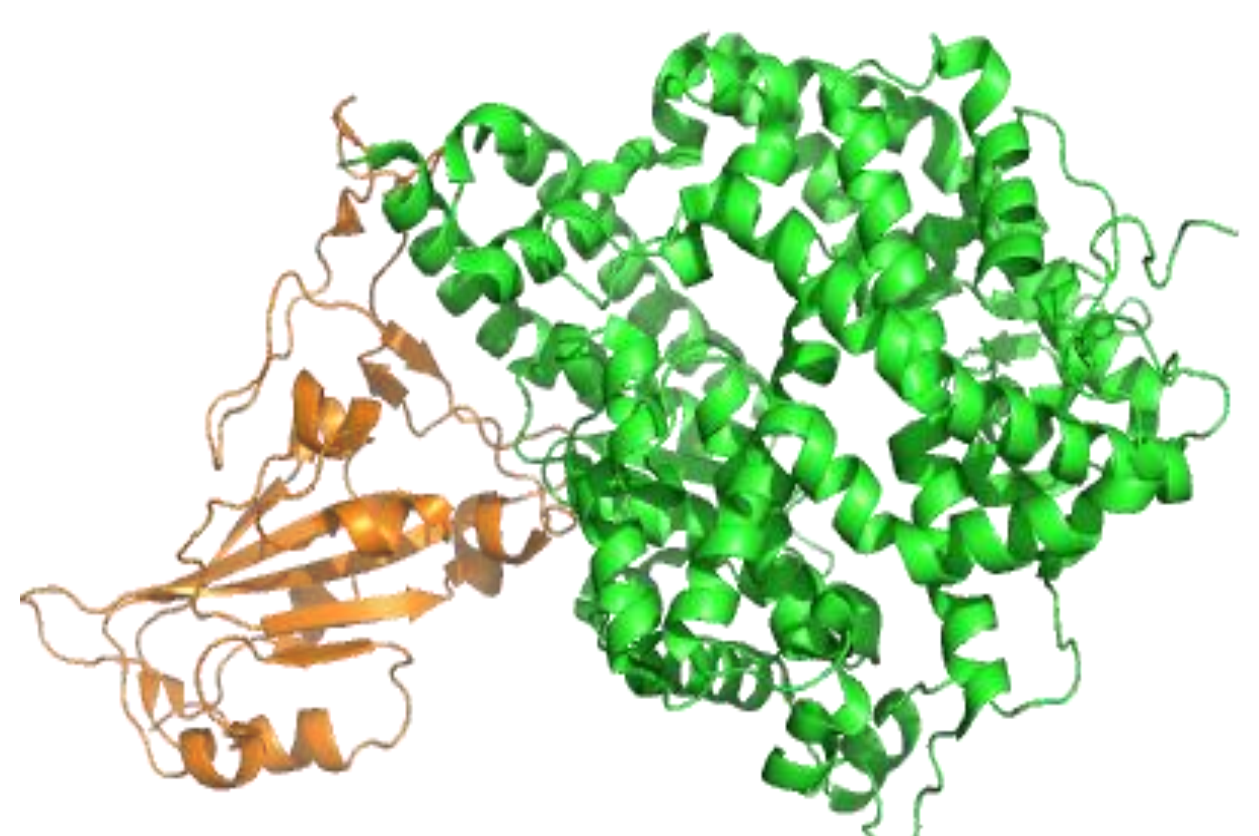
# EXPLORING IN SILICO PHARMACOLOGICAL ACTIONS OF PYRAMAX AGAINST SARS-COV-2

## Introduction

This study describes the basic steps and methodologies used in 'in silico' drug discovery. Based on the in vitro evidence that Pyramax inhibits the replication of SARS-CoV-2, this study systematically investigates the pharmacological potential of Pyramax using an 'in silico' approach.

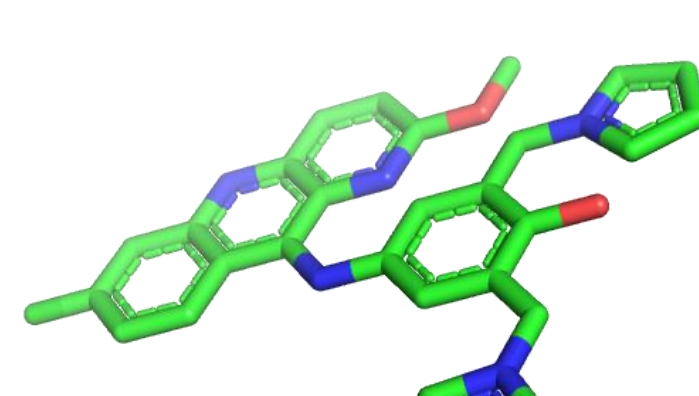
### <Drug Discovery>

- Protein target: 6MOJ
- SARS-CoV-2 spike receptor-binding domain bound with ACE2
- Consists of
  - The human angiotensin-converting enzyme (ACE2)
  - Viral spike protein S1

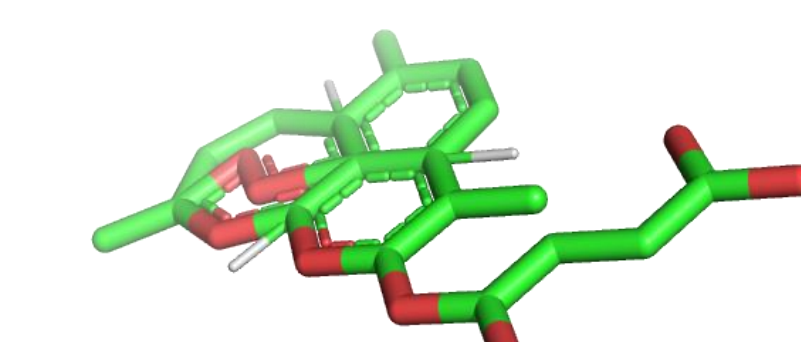


6MOJ

- Ligand/Drug target: Pyramax
- Antimalarial drug
- Consist of
  - Pyronaridine
  - Artesunate



Pyronaridine



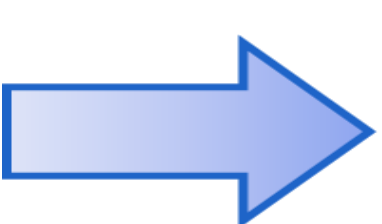
Artesunate



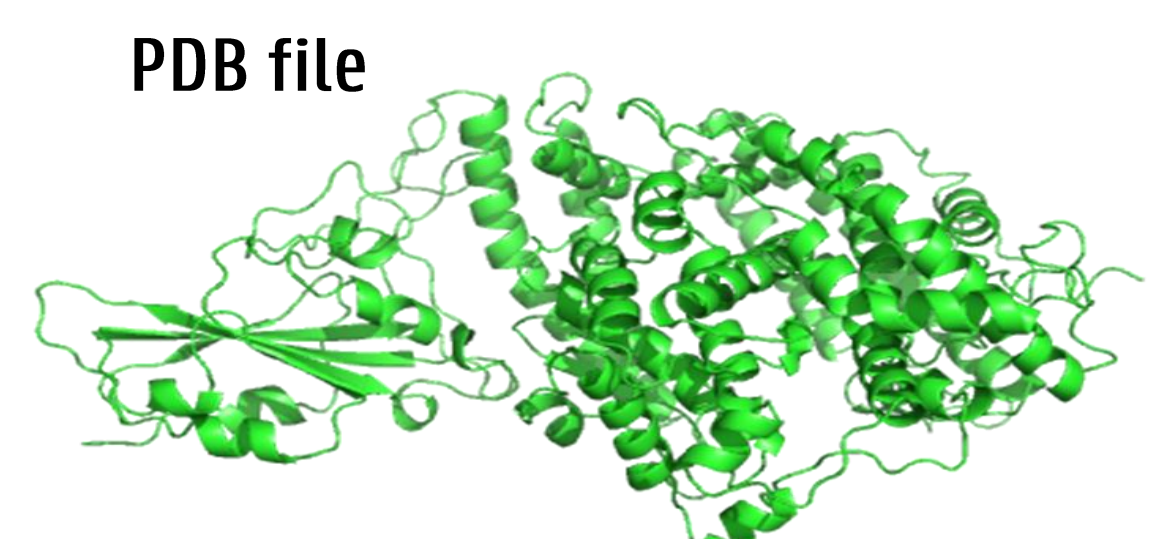
### <AlphaFold2>

- Predict the structure of the protein from the amino-acid sequence.

>FASTA file  
STIEEQAKTFLDKFNHEAEDLFY  
QSSLASWNYNTN....



PDB file

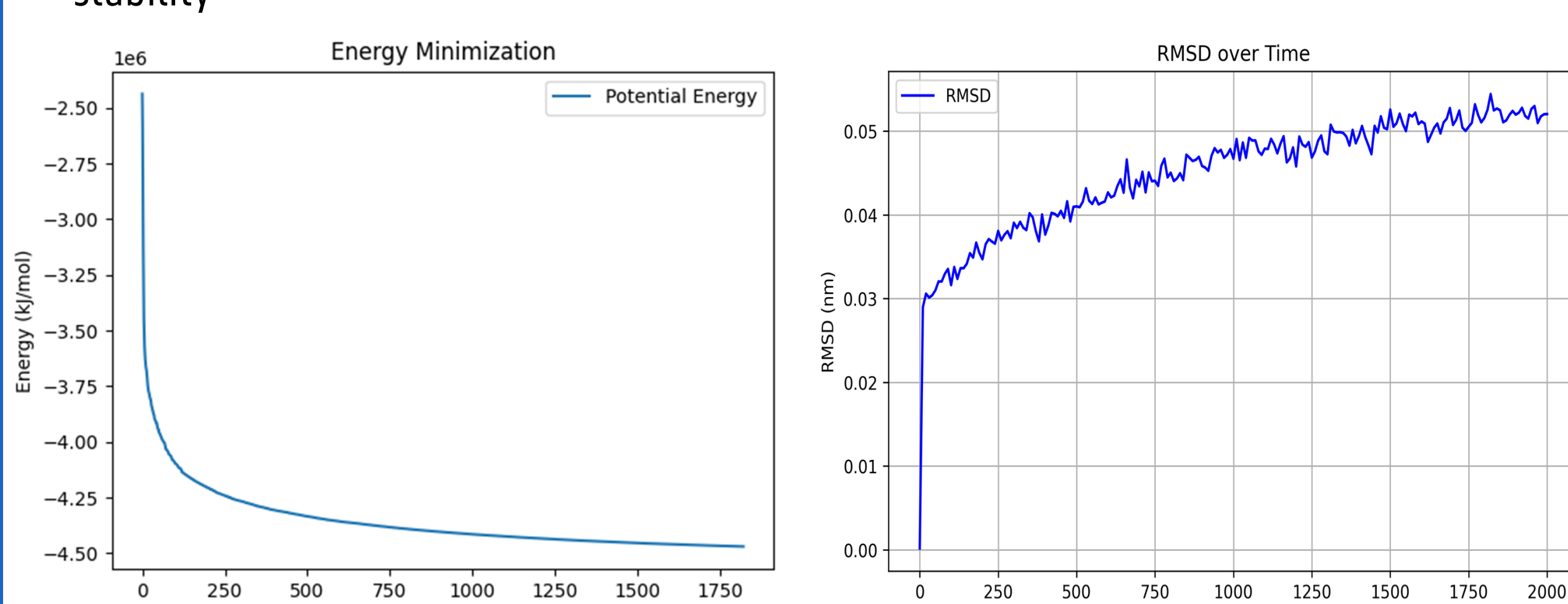


### <GROMACS>

- Key Components:
  - Force Fields: Mathematical models that define how atoms interact.
  - Integration Algorithm: Calculate changes in position and velocity over time.
  - Simulation Box: Defines the boundary conditions for molecular systems.

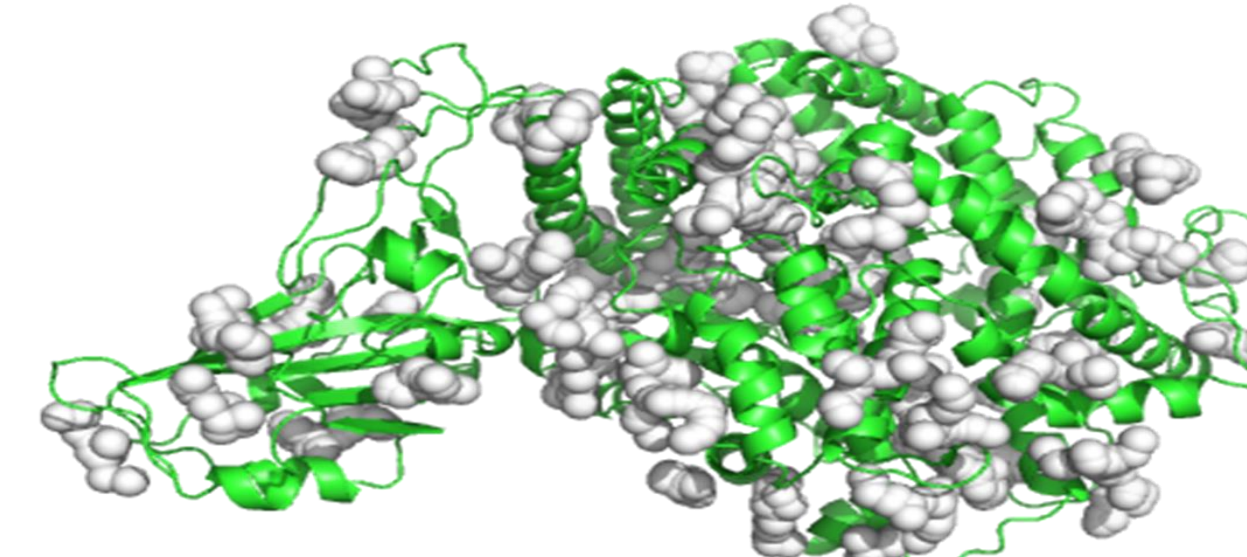
Component	Configuration
Force field	Protein AMBER14SB
	Ligand GAFF
Integration Algorithm	Velocity Verlet
Simulation Box	-d 1.0 -bt dodecahedron

- Energy Minimization:
- Process of minimizing the potential energy of a system to increase structural stability



- Predict the physically stable complex structure in terms of potential energy.
- RMSD remains stable state without significant structural deformation.

- Find all possible binding sites of the ligand on the protein.



- Determine the box-size & the center coordinate.

### <AutoDock>

- Inputs
- Protein pdb file
  - Ligand pdb file
  - Box size
  - Center coordinate

AutoDock

- Outputs
- Complex data
  - Binding Affinity

- Check the degree of the binding affinity for each sites.
- Find the best binding site in terms of binding affinity on each drug substance.

Binding Affinity ( $\Delta G$ , kcal/mol)	Interpretation & Drug-Like Potential
0 ~ -4 kcal/mol	Very weak binding, low drug potential
-4 ~ -6 kcal/mol	Moderate binding, require optimization
-6 ~ -8 kcal/mol	Good binding, potential drug candidate
-8 ~ -10 kcal/mol	Strong binding
< -10 kcal/mol	Very strong binding, promising drug lead

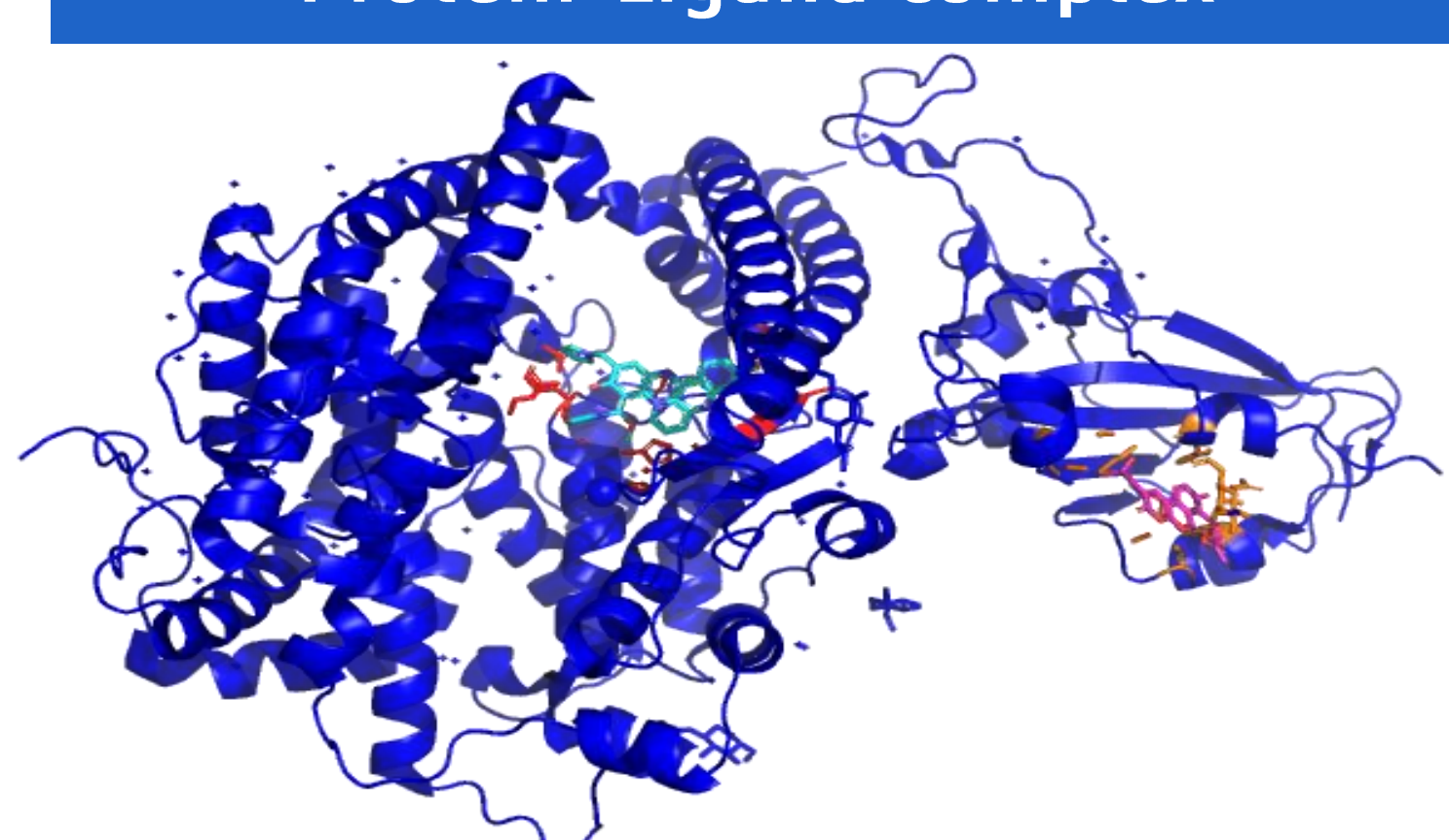
6MOJ-Pyronaridine Complex

Location	Affinity (kcal/mol)
1	-8.5

6MOJ-Artesunate Complex

Location	Affinity (kcal/mol)
11	-8.9

### <Protein-Ligand complex>



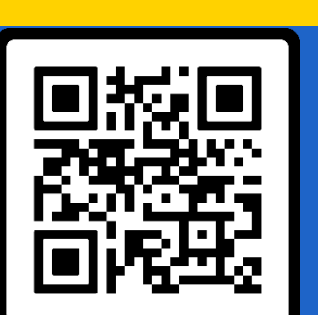
### <Further Analysis>

- Protein-Ligand Interaction Profiling
  - Analyze the binding-site amino acids.
- In silico ADMET Prediction
  - Predict and evaluate drug bioavailability.
- Clinical test
  - Application to human

### <Conclusion>

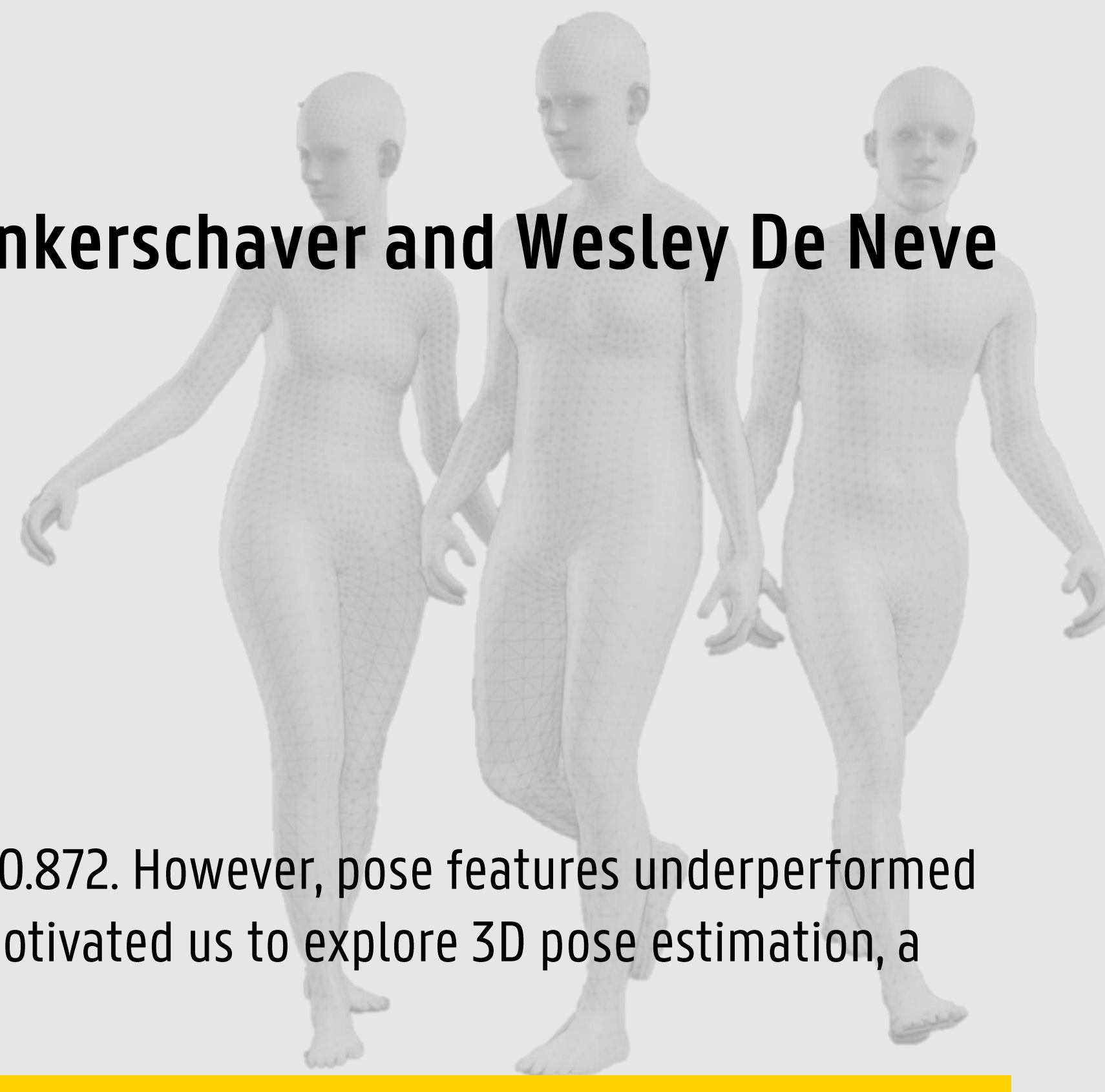
Pyramax substances exhibit high binding affinity to 6MOJ. The complex has been shown to possess high stability. Therefore, Pyramax is presumed to have strong potential for inhibiting the replication of SARS-CoV-2.

Contact  
Junseok.Kim@ghent.ac.kr



GitHub

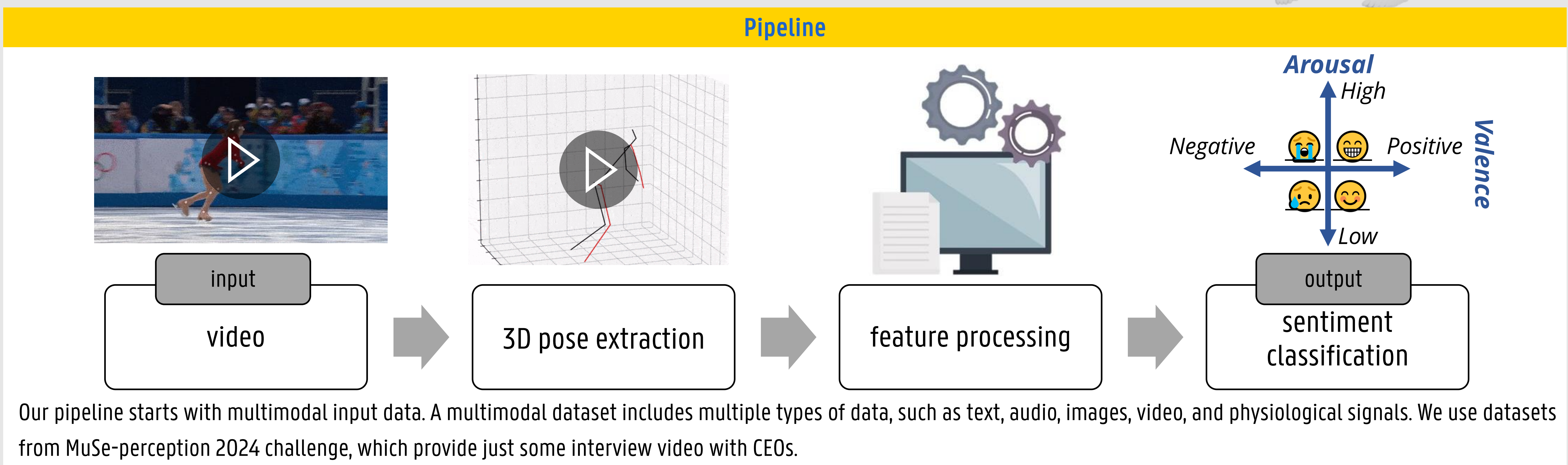




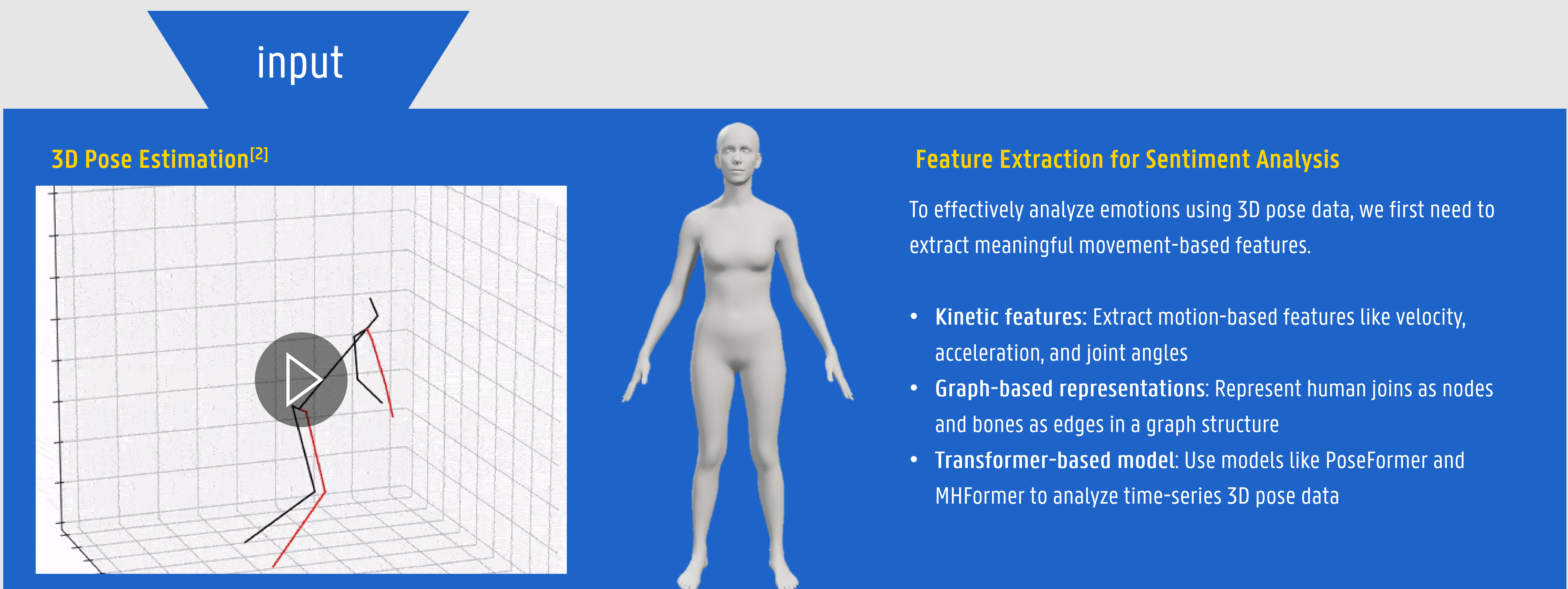
# 3D POSE ESTIMATION FOR ENHANCED SENTIMENT ANALYSIS: INSIGHT FROM THE MUSE CHALLENGE

## 3D Pose Estimation Enhances Sentiment Analysis

In our earlier research<sup>[1]</sup> for the MuSe-Stress 2022 challenge, we used a Transformer encoder model and achieved a combined CCC of 0.872. However, pose features underperformed compared to audio and video features. Despite hyperparameter tuning, model interpretability remained limited. These challenges motivated us to explore 3D pose estimation, a more informative and fine-grained representation, for better sentiment analysis.



Our pipeline starts with multimodal input data. A multimodal dataset includes multiple types of data, such as text, audio, images, video, and physiological signals. We use datasets from MuSe-perception 2024 challenge, which provide just some interview video with CEOs.



**3D Pose Estimation**

3D pose estimation is a computer vision technique that predicts the 3D spatial positions of human body joints, enabling more accurate motion analysis. 3D pose estimation adds depth information, enabling more accurate and realistic analysis of human motion. Common methods of 3D Pose are Estimation Direct 3D pose estimation, 2D-to-3D pose lifting, and SMPL model based estimations

**output**

Attributes	Confidence	Leadership	...	Warmth
Arousal / Valence	high / high	medium / low	...	low / high
predictability	82%	67%	...	58%

The most relevant attribute is Confidence (82%).

- Future Works**
1. Design and Implementation of a Multimodal Fusion Architecture
  2. Feature Engineering for Effective Representation
  3. Model Optimization and Interpretability Improvement
  4. Comprehensive Model Evaluation and Error Analysis

## Conclusion

Though in its early stage, the approach holds for broader use across affective computing applications.

## References

- [1] Park, H.-M., Kim, G., Van Messem, A., & De Neve, W. (2023). Muse-personalization 2023: Feature engineering, hyperparameter optimization, and Transformer-encoder re-discovery. Proceedings of the 4th on Multimodal Sentiment Analysis Challenge and Workshop: Mimicked Emotions, Humour and Personalisation, 89–97.
- [2] Pavllo, D., Feichtenhofer, C., Grangier, D., & Auli, M. (2019). 3D human pose estimation in video with temporal convolutions and semi-supervised training. 2019 IEEE/CVF Conference on Computer Vision and Pattern Recognition (CVPR), 7745–7754.

## Contact

Narim.Kim @gent.ac.kr

Universiteit Gent

@ugent

Ghent University



presentation

# CRISPR-CAS13D SYSTEM

## EFFICACY PREDICTION USING DEEP LEARNING



The CRISPR-Cas13 system is a promising RNA-targeting tool for diagnostic and therapeutic applications. However, off-target effects, where Cas13 cleaves unintended RNA, remain a major challenge. These effects are influenced by the efficiency of the guide RNA (gRNA), as imperfect binding can lead to collateral cleavage. Predicting sgRNA efficacy is crucial for minimizing off-target issues. Machine learning models have been developed to enhance sgRNA targeting accuracy, reducing off-target cleavage and improving the specificity of the CRISPR-Cas13 system.

### Dataset

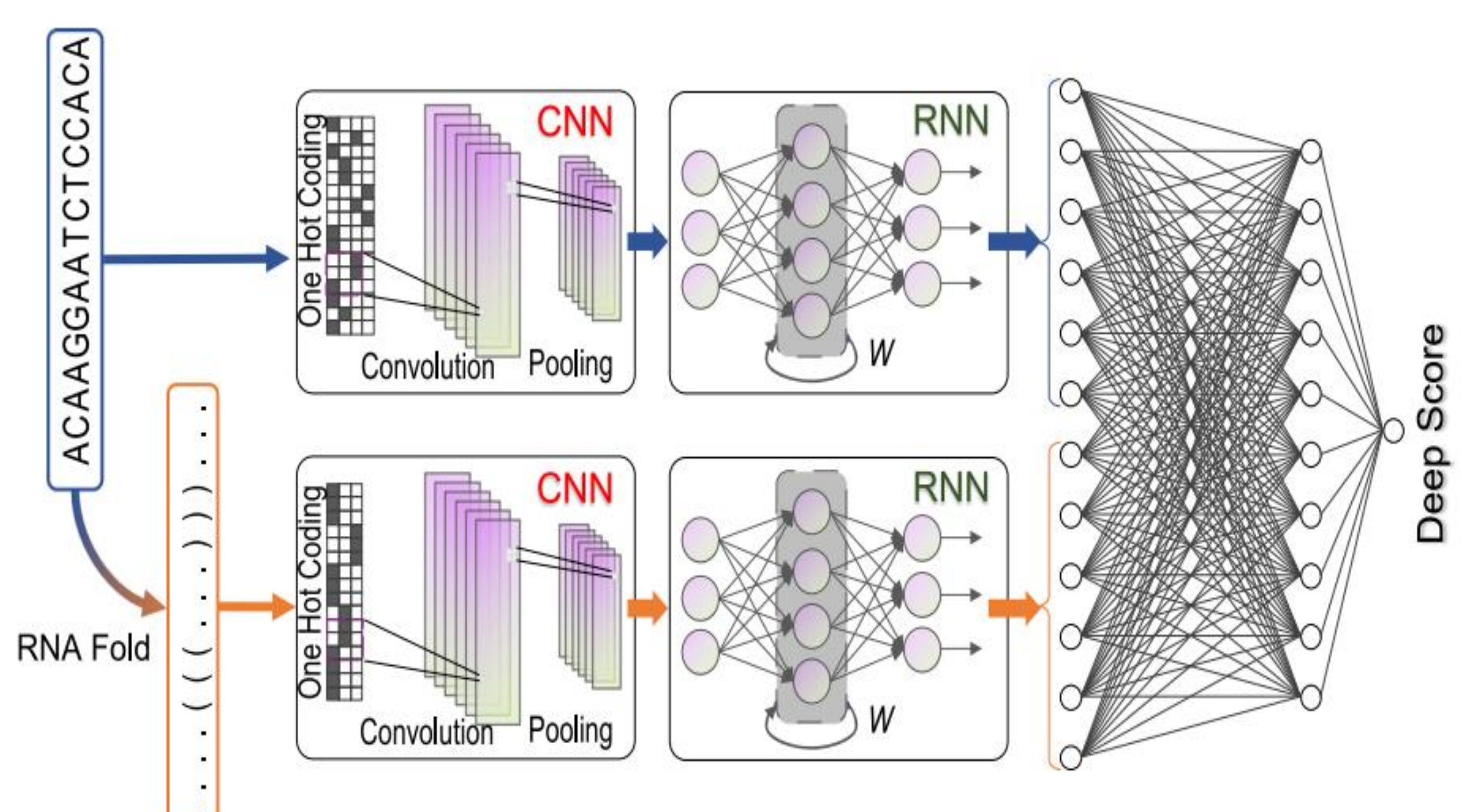
#### Original

	sgRNA	LFC	structure	MFE	DeepScore
0	CTGCAGGACAGGTGGCGTGGCCGAGCN	-0.016079	((....)).(((...)))).....	-7.2	0.319472
1	GCTGCAGGACAGGTGGCGTGGCCGAGCN	0.169027	.((....)).(((...)))).....	-7.3	0.141669
11	AAAGCATCCAGTGCTCAGGACAGGTGGCG	-0.271546	...(((((....))))....))..	-5.5	0.665170
12	CAAAGCATCCAGTGCTCAGGACAGGTGGCG	-0.190853	...(((((....))))....))..	-5.3	0.557433
13	CACAAAGCATCCAGTGCTCAGGACAGGTGGC	-0.441638	((....))).....))...	-4.2	0.838475

- 5726 samples
- Obtained from CRISPR screening experiment
- Log Fold Change (LFC):
  - (+) = up regulation of gene, (-) = down regulation of gene
  - $LFC \leq -0.5$  considered as an effective sgRNA
- For each sgRNA:
  - (1) secondary structure is calculated using ViennaRNA package
  - (2) efficacy score (= DeepScore) is calculated by normalizing LFC using customized sigmoid function
    - Ranges from 0 to 1
    - Designed to map effective LEC ( $\leq -0.5$ ) closer to 1

### CRNN Regression Model

#### (1) Model Architecture

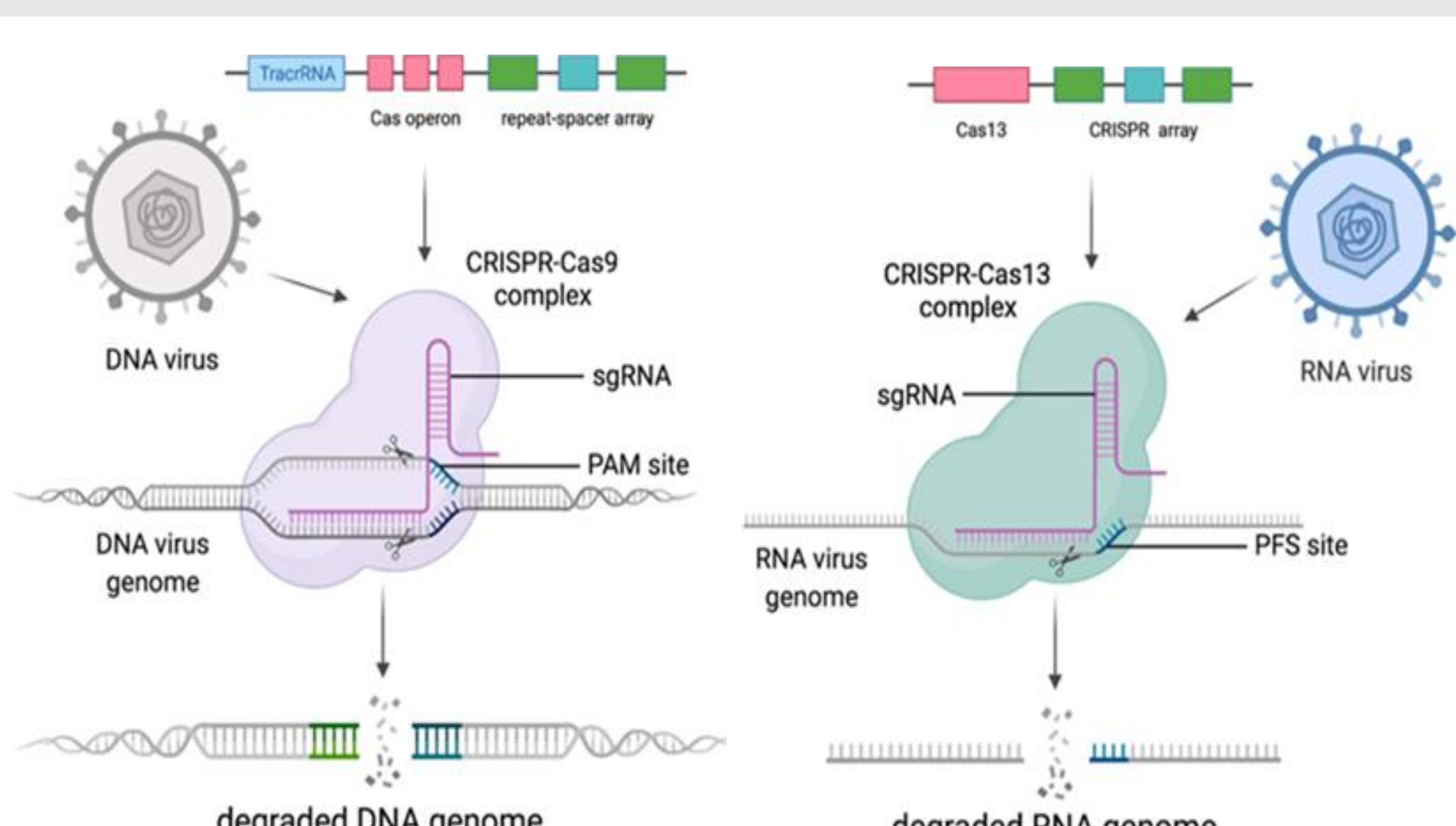


#### (2) Model Evaluation

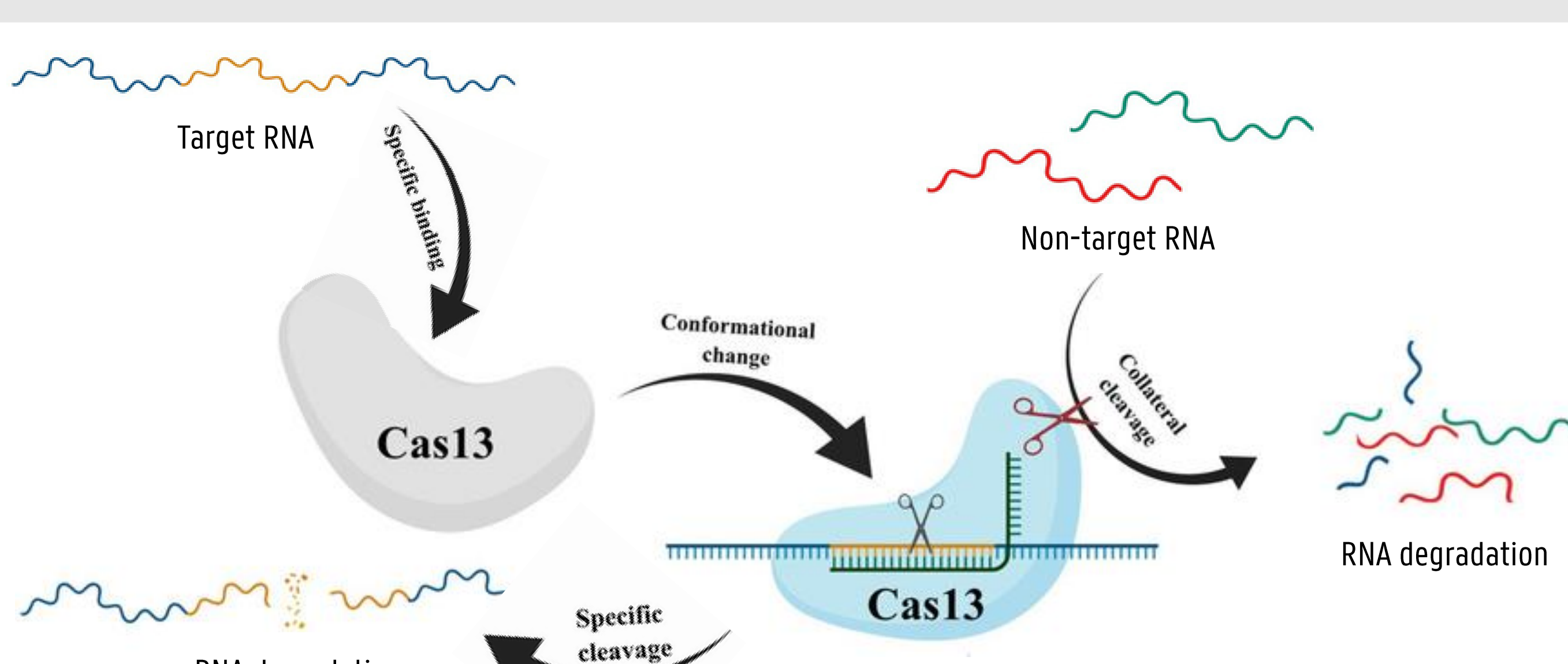
	MSE Loss	MAE	R <sup>2</sup>
CRNN	0.0700	0.2097	0.3786
SVR	0.0910	0.2615	0.1922
RFR	0.0952	0.2694	0.1549

- CRNN model shows the best performance with the lowest mean absolute error (MAE) and the highest coefficient of determination ( $R^2$ )
- All models exhibit low performance → need optimization

### CRISPR-Cas13 system

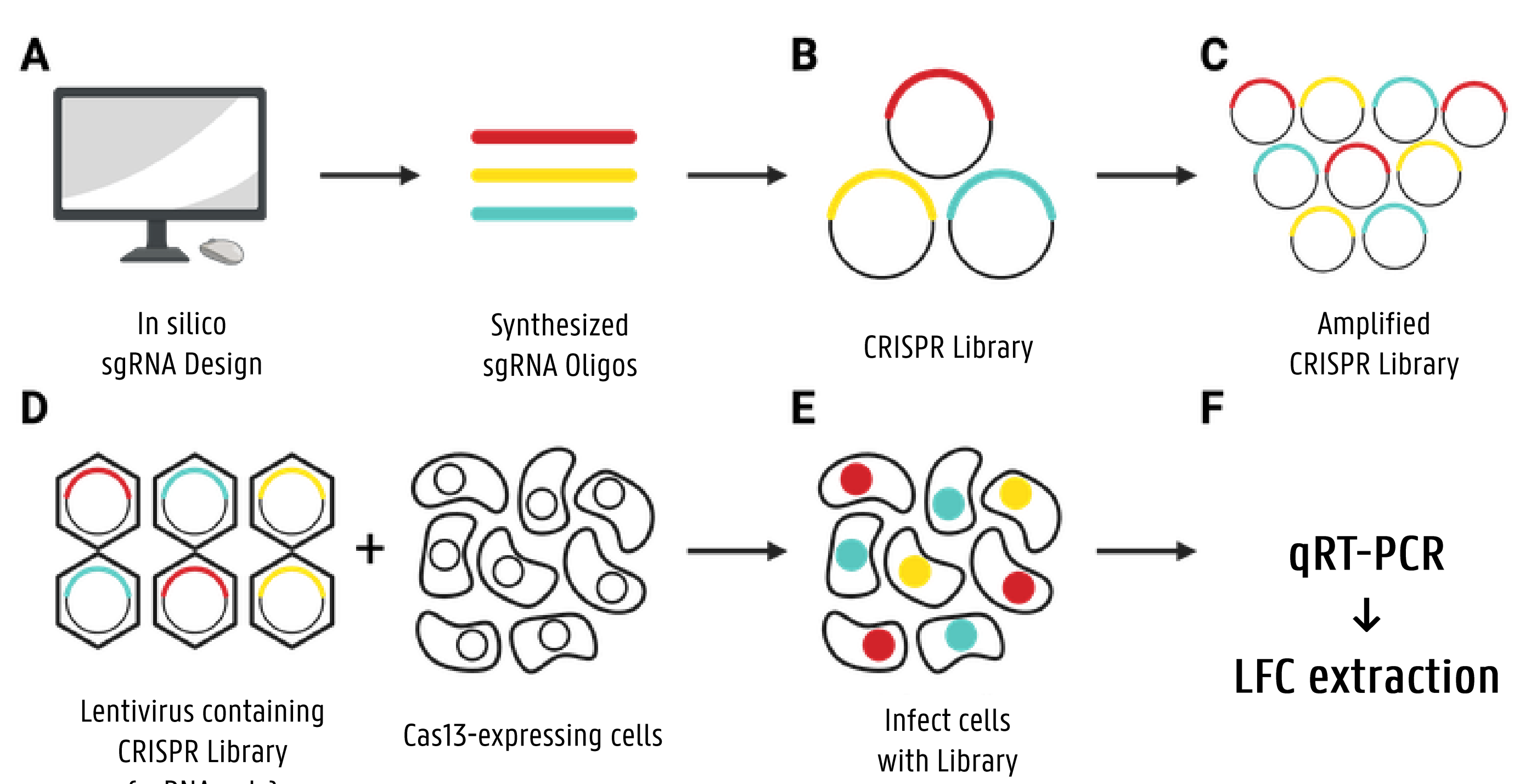


### Collateral Cleavage & Off-target Problem



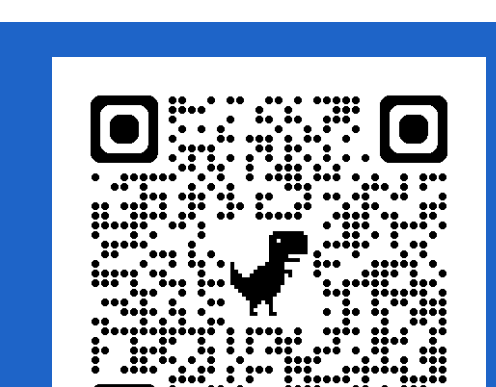
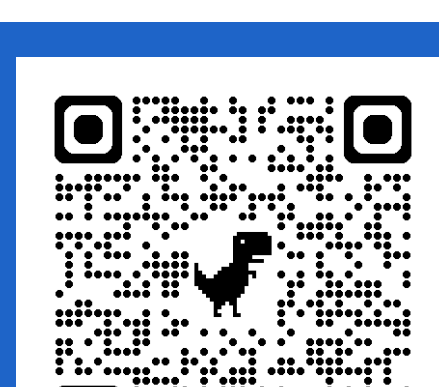
- Off-target effects hinder gene-editing & therapeutics
- Well-designed sgRNA minimizes off-target effects
  - CRISPR Screening needs trial-and-error
  - ML-based sgRNA efficacy prediction saves time and cost

### CRISPR Screening



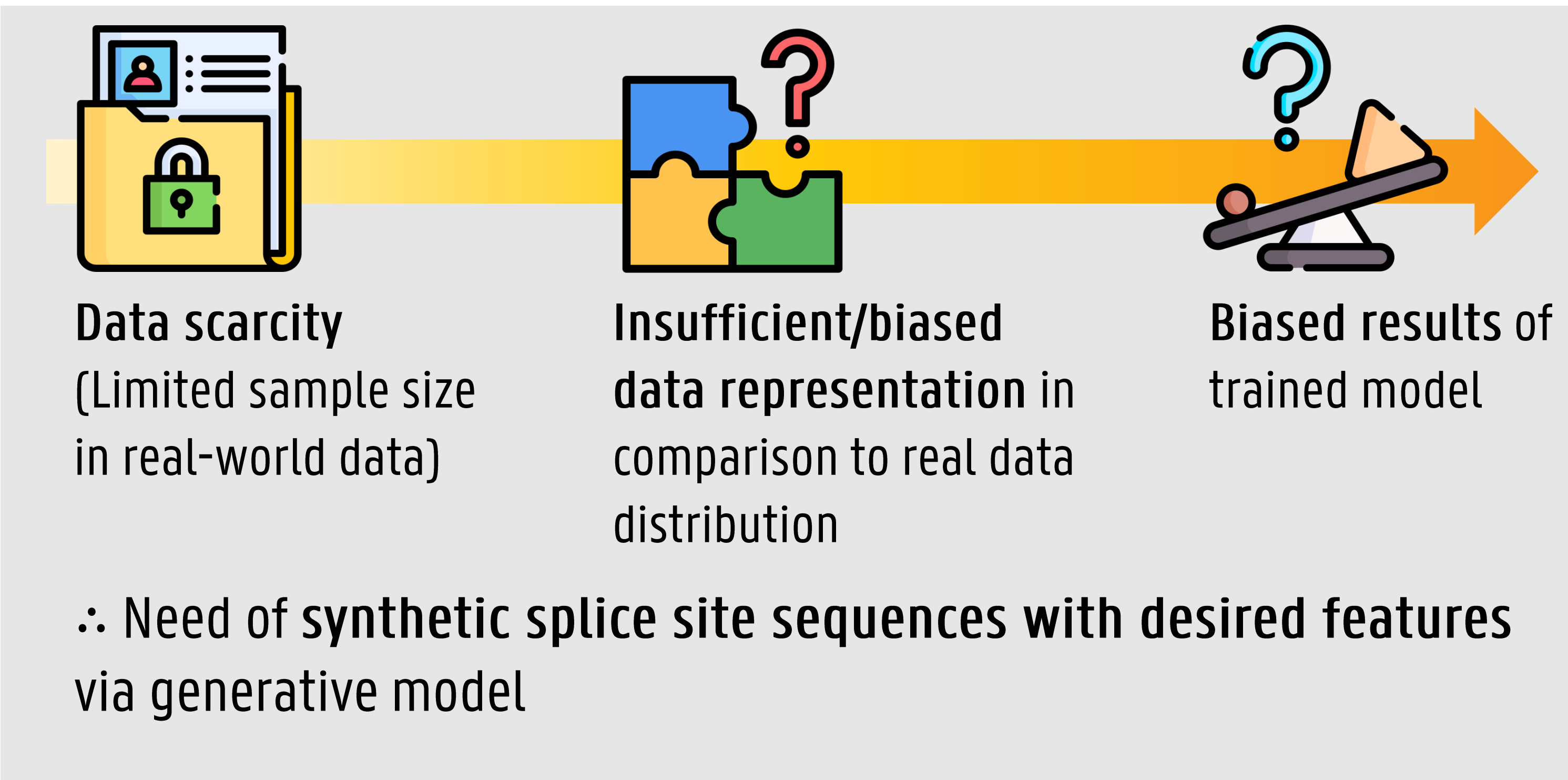
### Conclusion and Improvement

- CRNN model outperformed traditional regression models like SVR and RFR
- Hyperparameter fine-tuning (e.g., Grid Search) needed
- Incorporate target RNA structure/local sequence context (e.g., GC content)



# APPLICATION OF DIFFUSION MODELS TO SPLICE SITE GENERATION

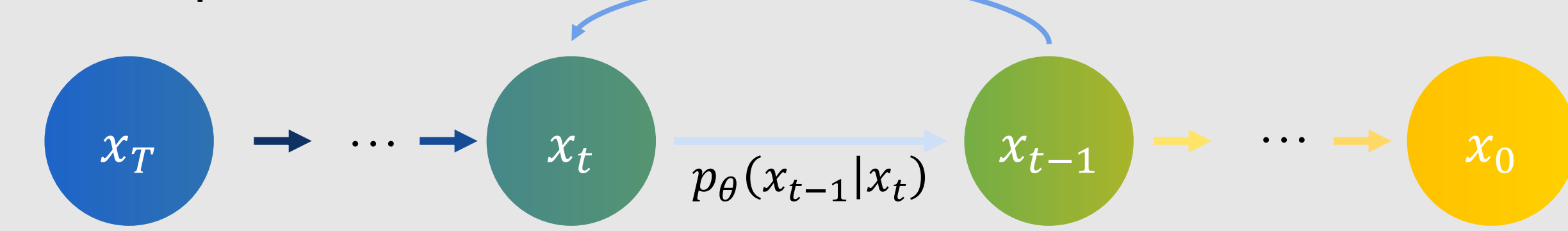
## Problems of Deep Learning in RNA Splicing



## Diffusion Models

Diffusion models were selected for its high diversity and fidelity of the generated samples, and because it is **robust to mode collapse problems**.

- **Forward process:** transforms an input  $x_0$  into a random noise  $x_T$ .
- **Reverse process:** noise removal from  $x_T$  to sample  $q(x_t|x_{t-1})$



**DNA Discrete Diffusion (D3):** generative framework for conditionally sampling regulatory sequences with targeted functional activity levels [1]

## Evaluation methods

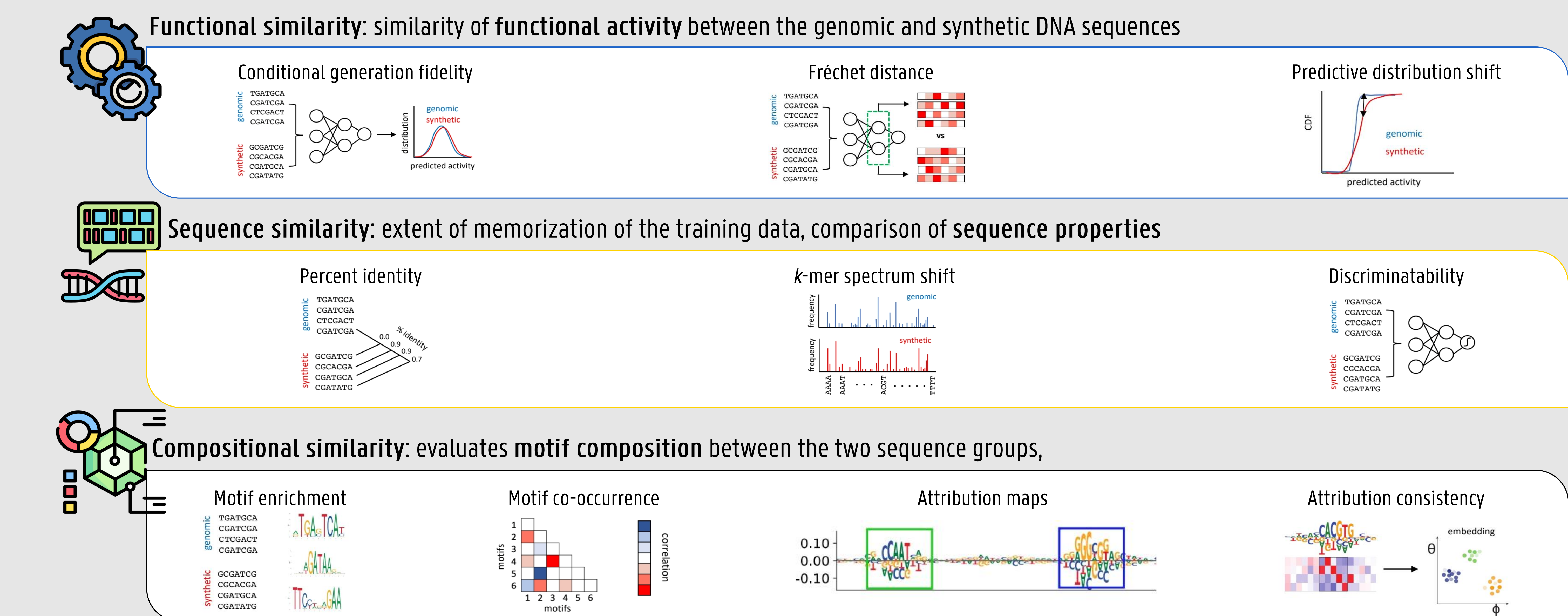


Figure 1. Summary of three main categories of the evaluation framework (Sarkar et al., 2024).

## Improved conditional sequence generation

Experiments	Human promoter	Fly enhancers	Cell-type specific MPRA	
Dataset	FANTOM database: 10,000 sequences (1024nt)	STARR-seq: 402,296 training, 40,570 validation, 41,186 test (249nt)	Dataset by Gosai et al: 640,029 training, 59,697 validation, 63,958 test (200nt)	Based on the evaluate framework suggested above, the model was tested upon three types of dataset: human promoter, fly enhancers and cell-type specific MPRA. The sequences generated by D3-based models have demonstrated <b>high diversity</b> and <b>high fidelity</b> in comparison to other conventional models as shown in the table.
Result	Conditional generation fidelity	▼	▼	
	Fréchet distance	-	▼	
	Predictive distribution shift	▼	▼	
	Percent identity	Low	-	
	k-mer spectrum shift	▼	▼	
	Discriminability (AUROC)	-	Closest to 0.5	
	Motif enrichment	▲	▲	
	Motif co-occurrence	▼	▼	
	Attribution consistency	-	▲	
	Attribution map	Figure 2. Overview of experiments with D3-based models in comparison to the conventional models.	Similar to real seq.	

## Reference

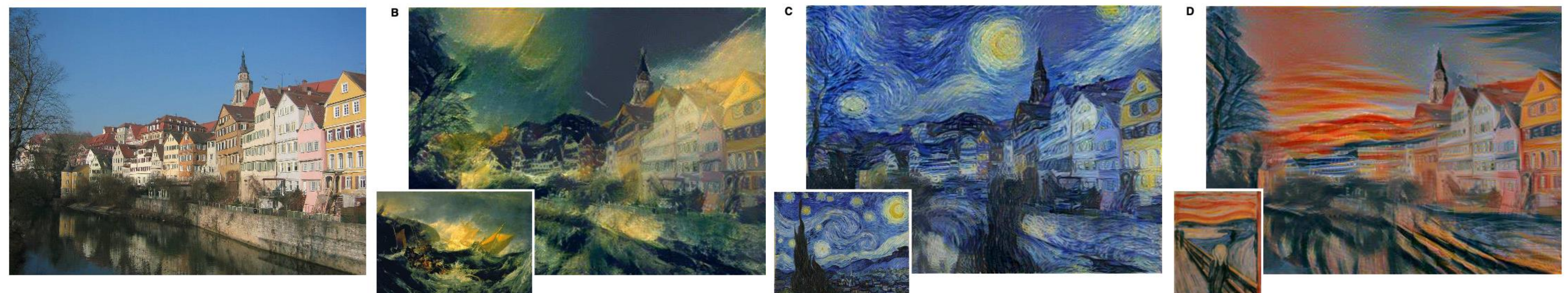
- [1] *Background: What is a Generative Model?* (2022, July 18). Google for Developers. <https://developers.google.com/machine-learning/gan/generative>
- [2] Sarkar, A., Tang, Z., Zhao, C., & Koo, P. (2024). Designing DNA With Tunable Regulatory Activity Using Discrete Diffusion. <https://doi.org/10.1101/2024.05.23.595630>
- [3] Vahdat, A., & Kreis, K. (2022, April 26). Improving Diffusion Models as an Alternative To GANs, Part 1. NVIDIA Developer. <https://developer.nvidia.com/blog/improving-diffusion-models-as-an-alternative-to-gans-part-1/>

## Future Works

Following such current work, there remains further improvements and tasks to be done. Existing models will be replicated and applied to splice site dataset. Models will further be modified or created to generate splice site sequences.



# EXPLORING NEURAL STYLE TRANSFER: IMAGE STYLE TRANSFER USING CONVOLUTIONAL NEURAL NETWORKS



## Abstract

Neural style transfer (NST) is a technique that applies the artistic style of one image (style image) to another image (content image) while preserving the structural information of the content image. NST uses a pre-trained Convolutional Neural Network (CNN) model, VGG-19, to extract and separate content and style representations from images. The process involves minimizing a loss function that combines both content loss and style loss, using gradient descent to iteratively update a generated image.

## VGG-19 in NST

NST utilizes:

- No fully connected layers
- One high-level convolutional layer for content representation
- One convolutional layer from each level for style representation

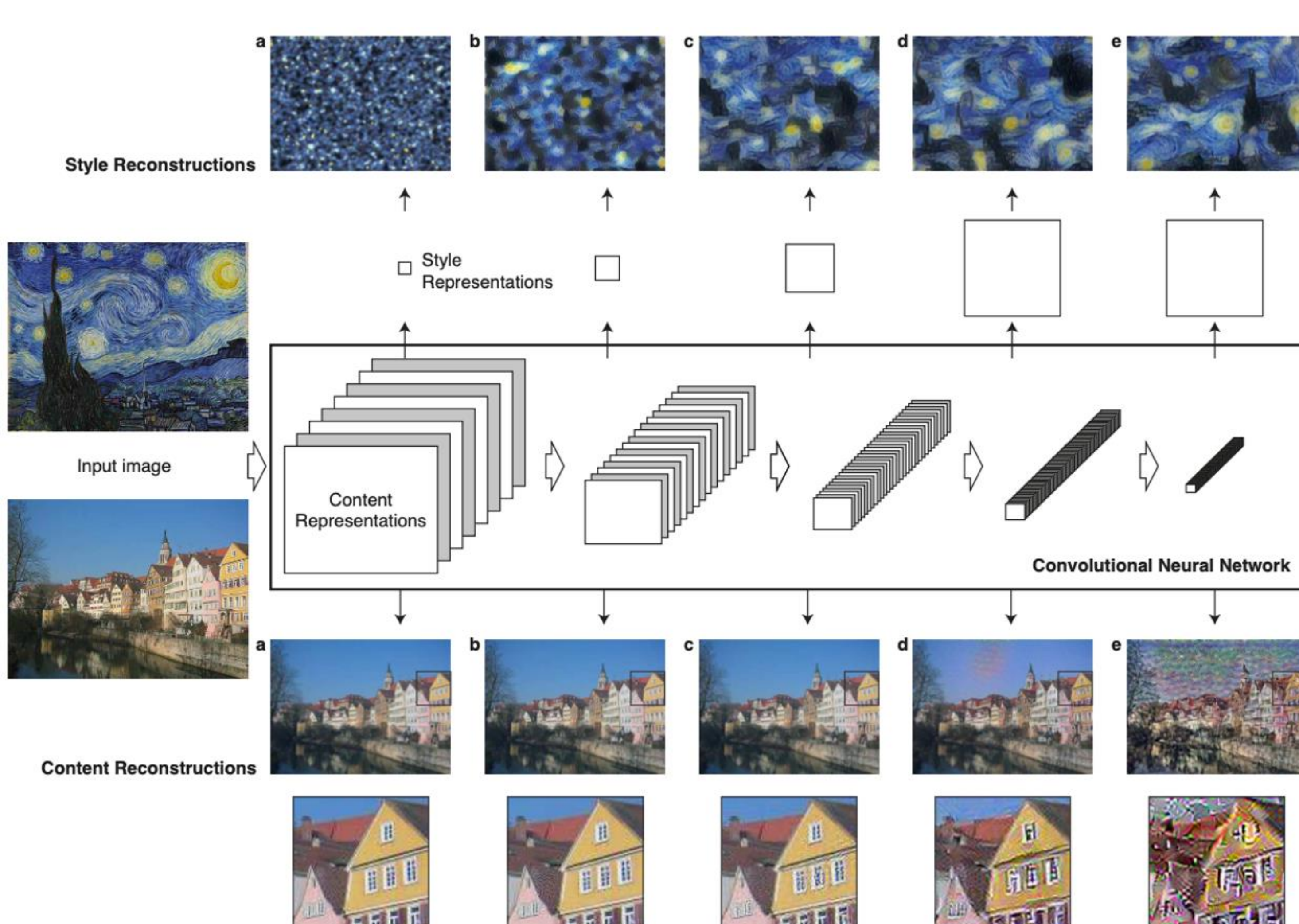


Figure 1. Visualization of feature representation contributions for different layers in VGG-19

Content reconstructions: (a) conv1\_1; (b) conv2\_1; (c) conv3\_1; (d) conv4\_1; (e) conv5\_1  
Style reconstructions: (a) conv1\_1; (b) conv1\_1, conv2\_1; (c) conv1\_1, conv2\_1, conv3\_1; (d) conv1\_1, conv2\_1, conv3\_1, conv4\_1; (e) conv1\_1, conv2\_1, conv3\_1, conv4\_1, conv5\_1

## Loss functions

$$L_{total}(\vec{p}, \vec{a}, \vec{x}) = \alpha L_{content}(\vec{p}, \vec{x}, l) + \beta L_{style}(\vec{a}, \vec{x})$$

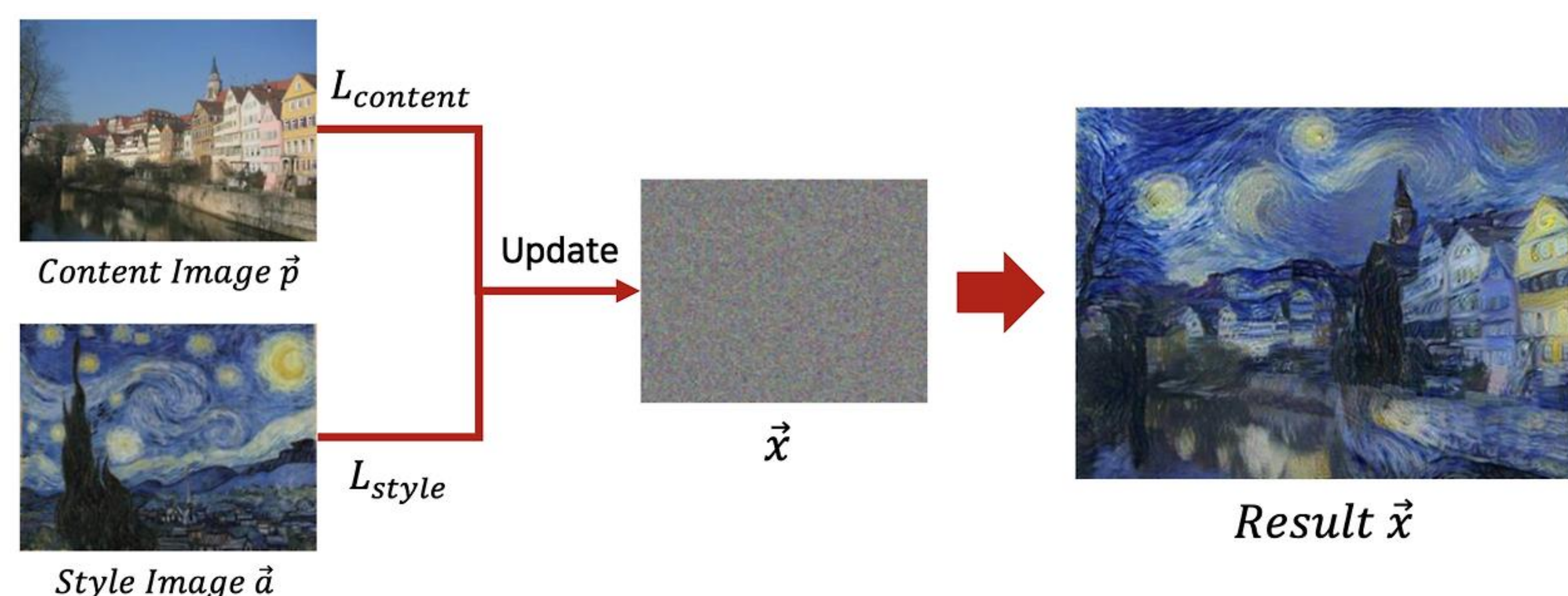


Figure 2. Basic mechanism of Neural Style Transfer

- $L_{total}$  : total loss
- $L_{content}$  : content loss
- $L_{style}$  : style loss

- $\vec{x}$  : white noise image
- $\alpha$  : weight for content loss
- $\beta$  : weight for style loss

## Content loss and style loss:

$$G_{ij}^l = \sum_k (F_{ik}^l F_{jk}^l)$$

$$L_{content}(\vec{p}, \vec{x}, l) = \frac{1}{2} \sum_{i,j} (F_{ij}^l - P_{ij}^l)^2$$

$$E_l = \frac{1}{4N_l^2 M_l^2} \sum_{i,j} (G_{ij}^l - A_{ij}^l)^2$$

$$L_{style}(\vec{a}, \vec{x}) = \sum_{i,j} w_l E_l$$

- $F^l, P^l$  : content representations of  $\vec{x}$  and  $\vec{p}$  in layer  $l$ ;  $F^l, P^l \in \mathbb{R}^{N_l \times M_l}$
- $N_l$  : number of feature maps in layer  $l$
- $M_l$  : size (width × height) of each feature map in layer  $l$
- $G^l, A^l$  : style representations of  $\vec{x}$  and  $\vec{a}$  in layer  $l$ ;  $G^l, A^l \in \mathbb{R}^{N_l \times M_l}$
- $E_l$  : contribution of each layer
- $w_l$  : weights of the contribution of each layer

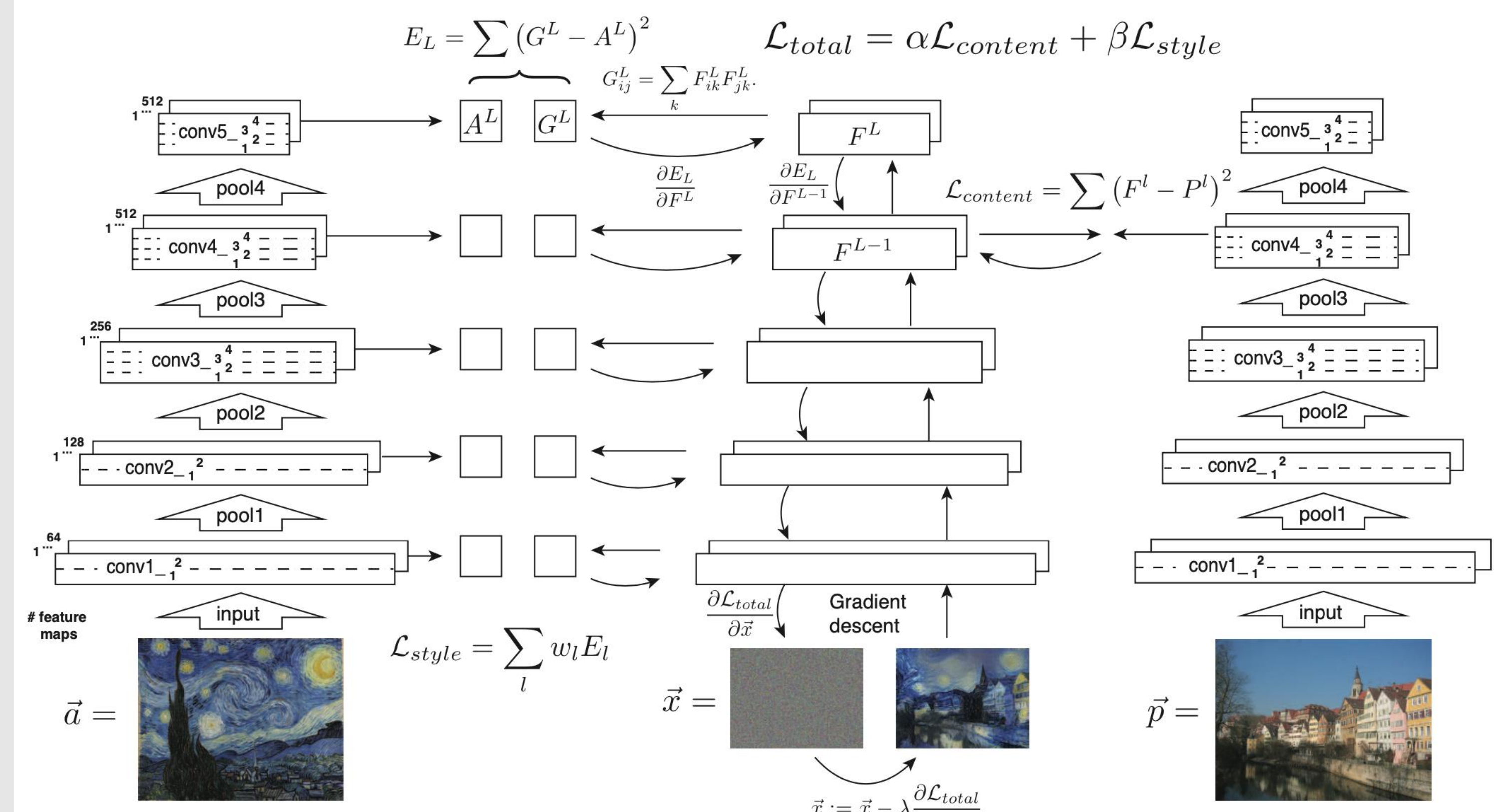


Figure 3. Overall training structure of Neural Style Transfer

## Observations



Figure 4. Trade-off between content and style matching based on different  $\alpha/\beta$  ratios  
With ratios of  $10^{-4}, 10^{-3}, 10^{-2}$ , and  $10^{-1}$  (from left to right)



Figure 5. Effect of different initializations on gradient descent  
From a content image, a style image, and random white noise images (from left to right)